JARO (2014)
DOI: 10.1007/s10162-014-0452-1

JARO
Journal of the Association for Research in Otolaryngology

Research Article

Three-Dimensional Vibration of the Malleus and Incus in the Living Gerbil

W. F. Decraemer,[1] O. de La Rochefoucauld,[2,6] W. R. J. Funnell,[3,4] and E. S. Olson[2,5]

[1]*Department Biomedical Physics, University of Antwerp, CGB, Groenenborgerlaan 171, 2020, Antwerpen, Belgium*

[2]*Department Otolaryngology, Head and Neck Surgery, Columbia University, 630 West 168th Street, New York, NY 10032, USA*

[3]*Department Biomedical Engineering, McGill University, 3375 rue University, Montréal, QC H4B 2S5, Canada*

[4]*Department Otolaryngology-Head and Neck Surgery, McGill University, 3375 rue University, Montréal, QC H4B 2S5, Canada*

[5]*Department Biomedical Engineering, Columbia University, 630 West 168th Street, New York, NY 10032, USA*

[6]*Inserm UMrsS587, Place Amelie Raba Leon, 33076, Bordeaux, France*

Received: 23 August 2013; Accepted: 3 March 2014; Online publication:

ABSTRACT

In previous studies, 3D motion of the middle-ear ossicles in cat and human was explored, but models for hearing research have shifted in the last few decades to smaller mammals, and gerbil, in particular, has become a popular hearing model. In the present study, we have measured with an optical interferometer the 3D motion of the malleus and incus in anesthetized gerbil for sound of moderate intensity (90-dB sound pressure level) over a broad frequency range. To access the ossicles, the pars flaccida was removed exposing the neck and head of the malleus and the incus from the malleus-incus joint to the plate of the lenticular process. Vibration measurements were done at six to eight points per ossicle while the angle of observation was varied over approximately 30 ° to enable calculation of the 3D rigid-body velocity components. These components were expressed in an intrinsic reference frame, with one axis along the anatomical suspension axis of the malleus-incus block and a second axis along the stapes piston direction. Another way of describing the motion that does not assume an a priori rotation axis is to calculate the instantaneous rotation axis (screw axis) of the malleus/incus motion. Only at frequencies below a few kilohertz did the screw axis have a maximum rotation in a direction close to that of the ligament axis. A slight slippage in the malleus-incus joint developed with increasing frequency. Our findings are useful in determining the sound transfer characteristics through the middle ear and serve as a reference for validation of mathematical middle-ear models. Last but not least, comparing our present results in gerbil with those of previously measured species (human and cat) exposes similarities and dissimilarities among them.

Keywords: middle ear, ossicular, chain, motion, measurement

Abbreviations: AMP – Anterior mallear process; ISJ – Incus-stapes joint (“*incudostapedial joint*”); LPI – Lenticular process of the incus; LPM – Lateral process of the malleus; MRA – Instantaneous rotation vector with maximal length (“*maximal rotation axis*”); MIJ – Malleus-incus joint (“*incudomallear joint*”); NM – Neck of the malleus; PIP – Posterior incudal process; PF – Pars flaccida; SPL – Sound pressure level in decibel—$\mathrm{SPL} = 20 \times \log_{10}\left(p_{\mathrm{rms}}/p_{\mathrm{ref_{rms}}}\right)$ dB with $p_{\mathrm{ref_{rms}}} = 2.10^{-5}$Pa ; TARA – Time-averaged instantaneous rotation axis

Present address: O. de La Rochefoucauld, Unité Mixte de Recherche en Santé, 1120, Institut National de la Santé et de la Recherche Médicale, CHU Pellegrin, bat PQR 3, Place Amelie Raba Leon, Bordeaux, 33076, France.

Portions of this work were presented in “Measurement of the three-dimensional vibration motion of the ossicular chain in the living gerbil,” Proceedings of Mechanics of Hearing, Williamstown, MA, USA, 2011 and at the 35th Midwinter Meeting of the Association for Research in Otolaryngology, San Diego, CA, USA, 2012.

Correspondence to: W. F. Decraemer · Department Biomedical Physics · University of Antwerp, CGB · Groenenborgerlaan 171, 2020, Antwerpen, Belgium. wim.decraemer@uantwerpen.be

INTRODUCTION

In the last two decades, the choice of mammals used for hearing experiments has moved from popular hearing models such as cat to smaller animals such as gerbil, guinea pig, and mouse. Due to anatomical differences among the species and obvious differences in size, experimental data that are amply available for cat may not be applicable to these animal models. Easy to breed and to house, and having an ear that is relatively large for the animal's overall body size, the gerbil has become a popular animal model. The size of the ossicles in gerbil is about 2/3 of that in cat; the ratio of their ossicular mass is about 1:8. For middle-ear mechanics research, this means that even though we are still studying a three-ossicle middle-ear chain with similar gross anatomy, the dynamics of the system may be expected to be quite different.

In a previous study, we described how the motion of the stapes (in response to an acoustic stimulus in the ear canal) was measured through a posterior-inferior opening in the middle-ear cavity wall (Decraemer et al. 2007). In the present paper, we complement that study by measuring the malleus and incus motion through the opening obtained by removing the pars flaccida (PF) of the tympanic membrane. Both approaches allow measurements on anesthetized animals; in some cases, data were taken post mortem without obvious differences. During the experiments, measurements of the ossicular vibrations were performed at a set of points on the thicker parts of the ossicles using different observation angles, allowing calculation of the 3D components of the ossicular velocities. We have assumed rigid-body behavior of the ossicles, at least of the parts of the ossicles observed. We will show in the "RESULTS" section good agreement between experimental data and the theoretical fits which proves that this assumption holds well; only a minor bending at the neck of the malleus was observed at the highest frequencies (>30 kHz). The motion of the each ossicle can thus be described by three rotational and three translational velocities. For easier interpretation of these velocities, they are transformed to a suitable intrinsic reference frame. Since it turned out that the rotation axis did not coincide with the a priori-assumed anatomical rotation axis, we used the screw axis concept to determine which axis the ossicles really rotate about and how this axis varies with time throughout a stimulus cycle. In the past, we conducted very similar measurements in cat and on human temporal bones, which allows us to discuss similarities and dissimilarities in the dynamical behavior of these different ears.

Organization of the Paper

To facilitate the reading flow of the paper, we first sketch a road map of the content. After the usual "INTRODUCTION" and "MATERIAL AND METHODS" sections, we inserted a special "THEORY" section with an introduction to *rigid-body motion*, the development of a *criterion for rigid-body behavior*, and the basics of the *screw axis* concept.

From there, the paper follows the normal road with a "RESULTS" section with a major part on animations of motion of the ossicular chain at different frequencies, followed by "DISCUSSION" and "CONCLUSION" sections.

MATERIAL AND METHODS

We will keep this section short as we can refer to a previous study where we followed a surgical preparation and experimental strategy almost identical to that used here (de La Rochefoucauld et al. 2008).

Animal Preparation

The measurements presented were obtained from four young gerbils of 50 to 70 g. After sedation with ketamine, they were deeply anesthetized with sodium pentobarbital. Supplemental doses were given when necessary. A tracheotomy was performed to maintain a clear airway. The body temperature was maintained at 37 °C using an animal blanket with rectal probe and controller. The care and use of animals were approved by the Institutional Animal Care and Use Committee of Columbia University.

No special measures such as spraying water mist in the middle-ear cavity were taken to avoid drying during the experimental session. Whenever the animal was manipulated during an experiment, the middle-ear cavity was checked, and no signs of drying out of the preparation were observed; the surface of the ossicles kept their moist and glossy appearance throughout the experiment. Removing the PF provided indeed only a small opening to the middle-ear cavity, and, in addition, the bony part of the ear canal was kept intact. Substantial drying of the specimen would be expected to change the ossicular vibration velocities by more than their standard deviation (the standard deviation for similar measurements with this setup was discussed in Decraemer et al. 2007) and this was not observed over the time window of about 1.5 h necessary to complete all runs necessary for a complete 3D experiment. When a cadaver was kept overnight for a post mortem experiment, it was wrapped in a moist cloth and stored in a plastic bag in a refrigerator.

We did not take special measures to prevent middle-ear muscle contractions. We are quite confident that we can rule out their occurrence because (1) the gerbils were under deep anesthesia [Dong and

Olson (2006) applying the same anesthesia procedure assumed that barbiturate eliminates middle-ear muscle activity in gerbil]; (2) during the experiment, we constantly had the highly magnified image of part of the ossicle under study on a monitor screen and we never observed sudden changes in the position of the object; (3) the signal level which is maximized by carefully focusing the interferometer laser spot on the ossicle did not suddenly decrease with the onset of the sound; and (4) we did not see differences between live and post mortem recordings that could be caused by such contractions.

Stimulus and Data Acquisition

Malleus and incus motions were measured in response to sound delivered in an open-sound field by an earphone directed toward and placed close to the ear canal (within 12–15 mm), which was shortened up to its bony end. A probe-tube microphone measured the sound near the edge of the ear canal (de La Rochefoucauld et al. 2008). We used pure-tone stimuli that were stepped between 250 Hz and 50 kHz in frequency (in steps of 0.5 kHz between 0.25 and 15 kHz, and then in steps of 1 kHz) with sound pressure level (SPL) kept constant at 80 or 90 dB SPL.

Malleus and Incus Velocity Measurements

For the velocity measurements, we used a noncommercial heterodyne laser interferometer which is combined with an optical microscope (Khanna et al. 1996; Willemin et al. 1988) so that the focused laser beam coincides with the center of the image of the microscope; the microscope allows visualization of the object (malleus or incus) while the interferometer measures the vibration at the selected location.

The animal's body was supported, and its head was immobilized by firmly clamping a head holder, which was cemented to the exposed top surface of the skull, to a post affixed to the positioning system. The positioning device consists of three orthogonal translation stages and two large, nested goniometers that are precisely aligned to rotate the object about the point of focus of the laser beam.

Vibration of the malleus and incus was measured through the opening obtained after removing the PF (Fig. 1). Measurements were made at a set of about six to eight points on each ossicle, and this was repeated for five different observation angles. The ossicles are positioned deep within the middle-ear cavity, which restricted the change in observation angle of the vertical and horizontal goniometers to a range of about −15 to +15 °. During the rotation, the animal, sound driver, and probe microphone moved together as they were all mounted to the same post of the positioning system, keeping relative positions unchanged.

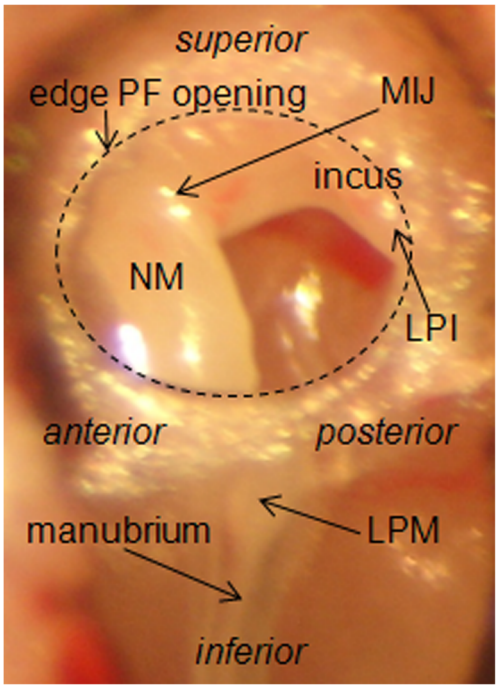

FIG. 1. When in gerbil the relatively large and nearly circular pars flaccida (*PF*) is removed, the part of the malleus between the lateral process (*LPM*) and the malleus-incus joint (*MIJ*), the neck of the malleus (*NM*), and the part of the incus from the MIJ to the long process of the incus (*LPI*) are exposed. This experimental approach also makes visible the superior part of the manubrium with the slightly outward bulging lateral process (*LPM*) in the external ear canal.

During each experiment, the motion of the bullar bone was also measured while the usual sound stimulus was played. This served as a check of the rigidity of the sample suspension and presented also a vibration "noise" floor. All measurements exceeded this level by at least 30 dB.

Rigid-Body Velocities in an Intrinsic Malleus-Incus Reference Frame

Ossicle by ossicle, the coordinates of all observation points and the observed velocities under all observation directions were used in one fitting procedure to calculate the 3D components of the rigid-body velocities, which describe the motion as the translation of a reference point on the body and the rotation of the body about this point. Details of the mathematical procedure are given in Decraemer et al. (2007).

These velocity vectors are expressed in the coordinate system used during the experiment. In this measurement frame, the object under study is quite arbitrarily oriented, which makes the physiological interpretation of the frequency responses of the

rotation and translation components almost impossible. Transforming these components into an object-related ("*intrinsic*") reference frame makes them more meaningful; for the gerbil, it happens that with the *x*-axis running from the tip of the anterior mallear process (AMP) to the posterior incudal process (PIP), we can align the *z*-axis to be parallel to the stapes piston direction (Fig. 2). Notice that this *x*-axis is also parallel to the stapes footplate. Let us call this *x*-axis the "anatomical rotation axis" since the suspension in the bulla at the ends of this axis clearly allows for rotation about this axis (see Fig. 2; de la Rochefoucauld et al. 2010) and call this frame the "anatomical frame". Let us recall that, classically, middle-ear motion was viewed as rotation about a fixed, anatomically defined axis, based on low-frequency experimental observations. Note that we do not use the term "ligament axis" as we used earlier for other species, as this implies a ligament at both ends of the axis; in gerbil, a thick ligament is present around the tip of the posterior incudal process, but on the mallear side, no ligamentous structure is observed where the tip meets the bullar wall (Rosowski et al. 1999) and the connection appears to be bony. The transformation matrix to express the rigid-body displacements in the intrinsic reference frame was determined by first registering a 3D model of the ossicular chain (constructed on the basis of a microCT scan of a complete gerbil temporal bone; Decraemer et al. 2003, 2007) with the experimental middle-ear orientation and then determining the transformation that brings the model into alignment with its position in the intrinsic reference frame. [It was not necessary to scan the temporal bones from all of the experimental animals because a comparison of models of five different animals (from some of our earlier experiments; comparison not published) showed that most gerbil middle ears were very similar in shape and size. Only one animal out of the five that we compared had somewhat smaller ossicles. Salih et al. (2012) found a similarly small variability for three gerbils.]

THEORY

Developing a Criterion for Rigid-Body Behavior

A basic assumption made in all of our subsequent analyses is that the ossicles behave as rigid bodies when set in motion by sound. The shift towards the use of smaller and smaller experimental animals, with middle-ear ossicles that are smaller and less massive but exposed to environmental sound fields of similar strength as the larger species, makes the question of whether the ossicles still move as rigid bodies more urgent. In this section, a simple criterion is developed to check whether a body moves rigidly.

Let us recall that the motion of a rigid body can be described by the translation of a reference point on the body with velocity $\mathbf{v}_{\text{trans}}$ and the rotation of the body about this point with angular velocity $\boldsymbol{\omega}$. The velocity of a point i of a rigid body in an inertial reference frame (e.g., a frame fixed to the earth) is then expressed as

$$\mathbf{v}_i = \mathbf{v}_{\text{trans}} + (\boldsymbol{\omega} \times \mathbf{r}_i) \tag{1}$$

In Eq. (1), r_i is the position vector of point i with respect to the reference point. A common experimental situation is that only one component—say the z component—of the velocity is measured, and from Eq. (1) we get

$$(\mathrm{v}_i)_z = (\mathrm{v}_{\text{trans}})_z + \omega_x y_i - \omega_y x_i \tag{2}$$

where $\omega_x y_i - \omega_y x_i$ is the z-component of $(\boldsymbol{\omega} \times \mathbf{r}_i)$.

We see that this component is not a function of z, the coordinate along the observation axis, but only of

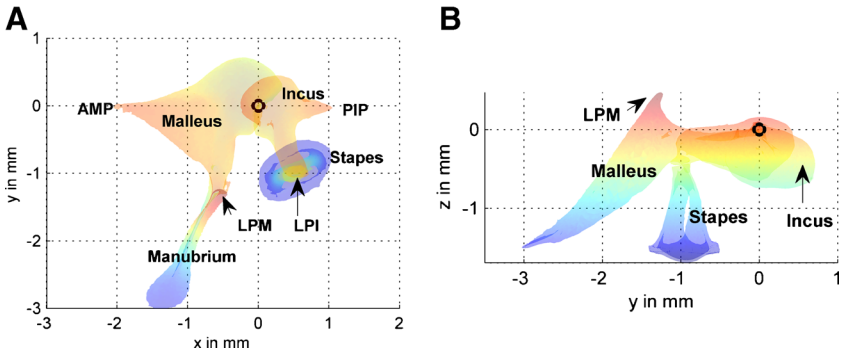

FIG. 2. Two views of the ossicular chain in the intrinsic reference frame that we adopted to express the malleus and the incus displacements. The *x*-axis is directed from the tip of the anterior mallear process (*AMP*) to the posterior incudal process (*PIP*) (**A**). The *z*-axis is along the stapes piston direction from the center of the footplate to the center of the stapes head as seen in **B**. The *y*-axis completes a right-handed reference frame. The origin, indicated with an *open circle* was chosen at the point where the *x*-axis crosses the malleus-incus joint (*MIJ*). The color code used for the ossicles in both panels goes from *blue* for small *z* to *red* for large *z* and can be evaluated in **B**.

x and y, the coordinates in the plane perpendicular to z, the *imaging* plane. As $(v_{trans})_z$ and ω_x and ω_y are *global*, i.e., the same for all points of the body and, thus, not functions of x, y, and z, it follows that they can only be functions of time t. Equation (2) tells us that, at a given instant of time, $(v_i)_z$ is linear in x and y, and thus when a 3D plot of $(v_i)_z$ as a function of x and y is made, all the points lie in one plane. If for example all observation points are aligned along the x-axis in the imaging plane (all y_i=0), then Eq. (2) simplifies further to

$$(v_i)_z = (v_{trans})_z + \omega_y x_i \tag{3}$$

indicating that now $(v_i)_z$ is a linear function of x. That is, *when velocities are measured on an ossicle at a set of points that are collinear in the imaging plane, a plot of the velocities as a function of position along the line must be a straight line if the ossicle is behaving rigidly*. While an ossicle is vibrating harmonically, $(v_{trans})_z$ and ω_y in Eq. (3) are also harmonic functions of time and this criterion must hold at each instant during the cycle. We will use this criterion to validate our assumption that the ossicles vibrate as rigid bodies during our experiments.

Let us finally remark that when we rewrite for example Eq. (2) as

$$\frac{dz_i}{dt} = \frac{dz_{trans}}{dt} - \frac{d\theta_x}{dt} y_i + \frac{d\theta_y}{dt} x_i \tag{4}$$

and multiply the left and right hand sides by dt, we obtain an equation for the infinitesimal displacements dz_i as a function of dz_{trans} and $d\theta_x$ and $d\theta_y$ (linear displacement in z of the reference point and angular displacements about the x- and y-axis, respectively):

$$dz_i = dz_{trans} - d\theta_x . y_i + d\theta_y x_i \tag{5}$$

With sound stimuli, the displacements are sufficiently small that all arguments developed for the velocities must also hold for the displacements.

Translation Displacement and Choice of Reference Frame

In the rigid-body motion description, the translation is the displacement of the origin of the reference frame, and the rotation is specified about this origin. When another origin O' is chosen, the new position coordinate of a given point can be written as $\mathbf{r'}_i = \mathbf{r'}_O + \mathbf{r}_i$ with $\mathbf{r'}_O$ being the position vector of the old origin O relative to O'. Using this in (1) yields

$$\begin{aligned} &\mathbf{v}_i = \mathbf{v}_{trans} + \boldsymbol{\omega} \times \left(\mathbf{r}'_i - \mathbf{r}'_O\right) \\ &\text{or} \quad \mathbf{v}_i = \left(\mathbf{v}_{trans} - \boldsymbol{\omega} \times \mathbf{r}'_O\right) + \boldsymbol{\omega} \times \mathbf{r}'_i = \mathbf{v}'_{trans} + \boldsymbol{\omega} \times \mathbf{r}'_i \end{aligned} \tag{6}$$

which means that the translation velocity in this new frame becomes

$$\mathbf{v}'_{trans} = \mathbf{v}_{trans} - \boldsymbol{\omega} \times \mathbf{r}'_O \tag{7}$$

while the rotation velocity remains unchanged. In other words, the choice of the reference frame determines the value of the rigid-body translation velocity (and thus also of the translation displacement).

Instantaneous Rotation Axis ("Screw Axis Concept")

We showed above that choosing a different origin for the reference frame, attached to and moving along with the body, results in a change of the rigid-body translation velocity [cf. Eq. (7)]. The term describing the change, $-\boldsymbol{\omega} \times \mathbf{r'}_O$, is a vector perpendicular to the rotation vector $\boldsymbol{\omega}$, and it is possible to choose an origin so that this term cancels the component of $\mathbf{v}_{trans}$ perpendicular to $\boldsymbol{\omega}$. This leaves us with a motion that is now described by the rotation $\boldsymbol{\omega}$ executed about the new reference point, and a translation ("*slide*") which takes place along the rotation vector $\boldsymbol{\omega}$, which is then called the "*screw axis*". In describing the displacement that brings the body from its rest position into its displaced position at an instant of time t, this axis can also be seen as an "*instantaneous rotation axis*". (The introduction to the screw axis concept given here should be sufficient to understand the screw axis discussion in the present paper. For further reading, one could consult Wikipedia or a book on basic kinematics such as Angeles (1982) and Bottema and Roth (1979)).

The spatial location of the screw axis is usually specified by an anchor point with position vector $\mathbf{R}_0$, the normal from the origin onto the screw axis. When an object performs an arbitrary 3D motion (e.g., a coin tossed up in the air), the instantaneous rotation axis changes from instant to instant, and the point $\mathbf{R}_0$ follows a path in 3D space. For an ossicle that vibrates harmonically with instantaneous rotation axes that vary in direction and location with time, the path of $\mathbf{R}_0$ is an ellipse.

RESULTS

In line with our previous papers, the motion of the ossicles will be specified in terms of displacements

rather than velocities as it makes interpretation and visualization of the mode of vibration easier. Displacement amplitudes and phases in the following sections are all expressed relative to the simultaneously recorded sound pressure measured near the entrance to the EC.

Verification of the Rigid-Body Criterion for Malleus and Incus

To check for rigidity, a set of observations on collinear observation points is required. This was not readily available as, during the experiment, the choice of observation points was guided by the desire for a high interferometer carrier level (the stronger the carrier, the lower the noise level and hence the smaller the experimental error) and geometrical accessibility; for the incus, for example, it was impossible to measure at collinear points due to its particular geometry and the limited access via the PF opening. Figure 3 indicates the locations of the observation points on the malleus (red dots) from the lateral process of the malleus (LPM) to the vicinity of the malleus-incus joint (MIJ), and for the incus (green dots) from the incus edge of the MIJ to the lenticular process of the incus (LPI) (animal 9d8 experiment); we see that the measurements points are not collinear. Fortunately, the observed displacements are smooth functions of x and y without sudden jumps or local extrema, so a spatial interpolation of the displacement data was a safe procedure to provide a set of velocities at points (shown in blue, between the LPM and the MIJ for the malleus, and between the MIJ and the LPI for the incus) that are collinear (the need for which is discussed above in the section "Developing a Criterion for Rigid-Body Behavior" and equidistant (which is not necessary, but is convenient). The interpolation was done separately on the real and imaginary parts of the displacement, and, afterwards, these were reconverted to amplitude and phase. Interpolation was performed using the "linear" method of the MATLAB (MathWorks) function TriScatteredInterp. In Fig. 4, the displacements of the interpolated collinear "observation" points on the malleus are plotted as a function of position for seven instants of time during the cycle (0, T/7, 2T/7… and 6T/7, labeled 1 to 7) for animal 9d8 to check the rigid-body criterion formulated in the previous section. Results for three frequencies (low, mid, and high values, annotated at the top) are shown in three panels: the blue circles connected by the solid blue line represent the interpolated experimental data, and the solid straight line in red shows the rigid-body fit to the blue data points. The fit was extrapolated (dashed red line) to the point with zero displacement, which represents the point about which the instantaneous rotation takes place (open red circle). Figure 5 shows a similar plot for the observations on the incus. For both the malleus and the incus, the linearity of the displacement-versus-position plots at all instants of time shown is striking for the low and mid frequencies. At the higher frequencies, the blue lines deviate slightly from linear indicating some bending of the ossicle, but, nevertheless, the rigid-body assumption remains valid as a good approximate description. Strong departures from rigidity were not seen during the present experiments as the parts of the malleus and incus observed are solid compared with the manubrium tip, where higher vibration modes were observed earlier (Decraemer et al. 1994; de La Rochefoucauld et al. 2010). The bending seen here also occurred at relatively thinner and hence more flexible parts of the ossicles, the neck for the malleus and partway along the long process for the incus (cf. Figs. 1 and 2).

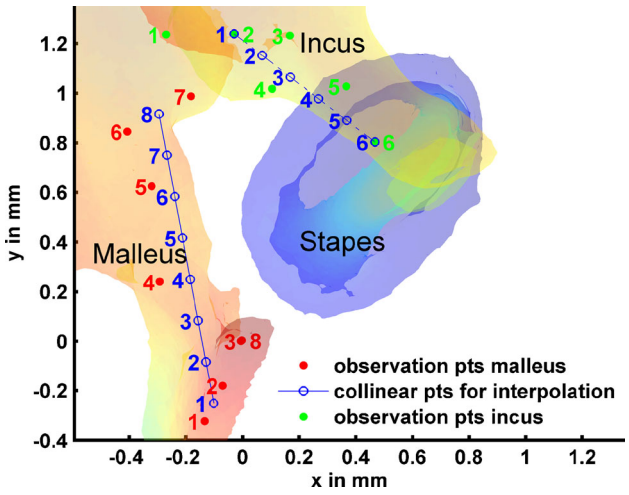

FIG. 3. Observation points on the malleus (*red*) and the incus (*green*) in the experimental reference frame (which was close to, but not exactly equal to the intrinsic frame of Fig. 2). To obtain displacement observations at collinear points, a spatial interpolation was performed at collinear points (*blue*) on the malleus and incus, respectively (example shown for animal 9d8).

GOODNESS OF FIT

In Fig. 6, we illustrate the good quality of the rigid-body fit to the experimental data over a wide frequency range by comparing the experimental amplitude and phase at a few observation points on the malleus and incus (locations shown in inset) as a function of frequency to the fit obtained by the rigid-body model. Although the fit makes use of the observations at all the different observation angles used during the entire experiment, we make a direct comparison here between experiment and model for observations at a few selected points on the malleus and incus for one observation angle.

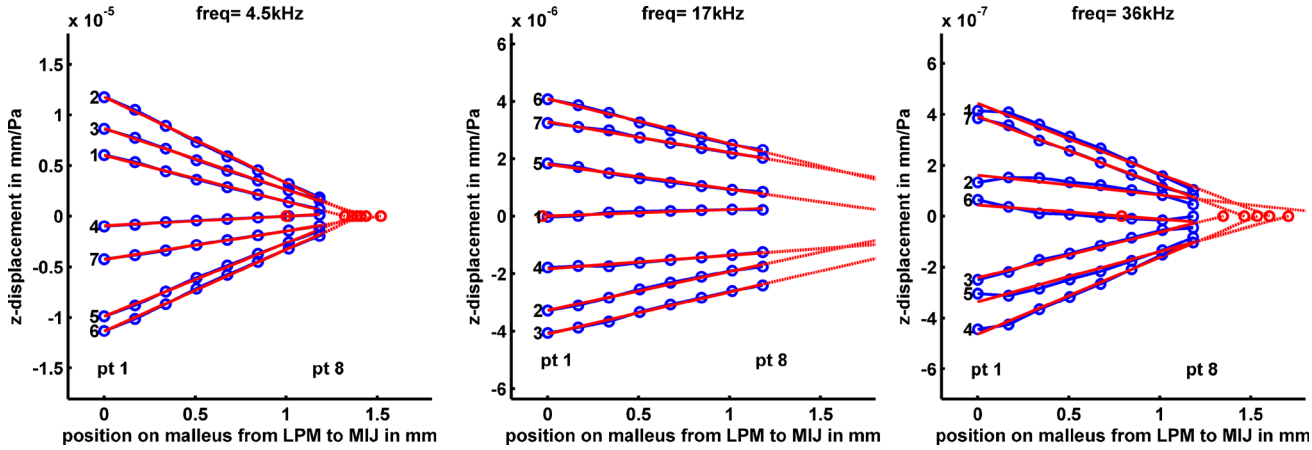

FIG. 4. Displacements of the eight interpolated points on the malleus between the LPM and MIJ shown in Fig. 3 (animal 9d8) for seven equally spaced phases in a cycle (annotated one to seven) plotted as a function of position (*blue circles*); *left panel* 4.5 kHz, *middle panel* 17 kHz, and *right panel* 36 kHz. Note that the mode of vibration changed with frequency. In *red,* a rigid-body fit to the experimental data is shown. The displacements at the "experimental points" (obtained after spatial interpolation to get collinear points) align nearly perfectly with the straight line segments of the rigid-body fit, except for the highest frequency where a small deviation from linearity in the region of the malleus neck suggests some bending. The point where the line crosses the *x*-axis can be considered as an instantaneous rotation point.

The experimental displacements for the malleus and incus of animal 11d8 observed at a mid-range observation angle (allowing goniometer rotation in both directions) are shown in Fig. 6A (amplitude normalized by sound pressure) and Fig. 6B (phase relative to sound pressure) using different-colored dots (see legend of Fig. 6) for each observation point. The rigid-body fit for each point is shown as a solid line using the same color code. We see that at most frequencies, the agreement between the amplitudes and phases of experiment and fit is very good for all the locations. For the point at the neck of the malleus (red), the agreement is somewhat worse at the highest frequencies, probably caused by the bending seen in this region in Fig. 4. For the incus, the point near the MIJ (blue) also shows minor discrepancies in the 20- to 40-kHz region; this point had the smallest amplitude, and, consequently, the effects of any experimental error could have been somewhat larger.

RIGID-BODY ANALYSIS RESULTS

We showed above that the motion of a rigid body can be completely described by a whole-body translation in combination with a whole-body rotation. The

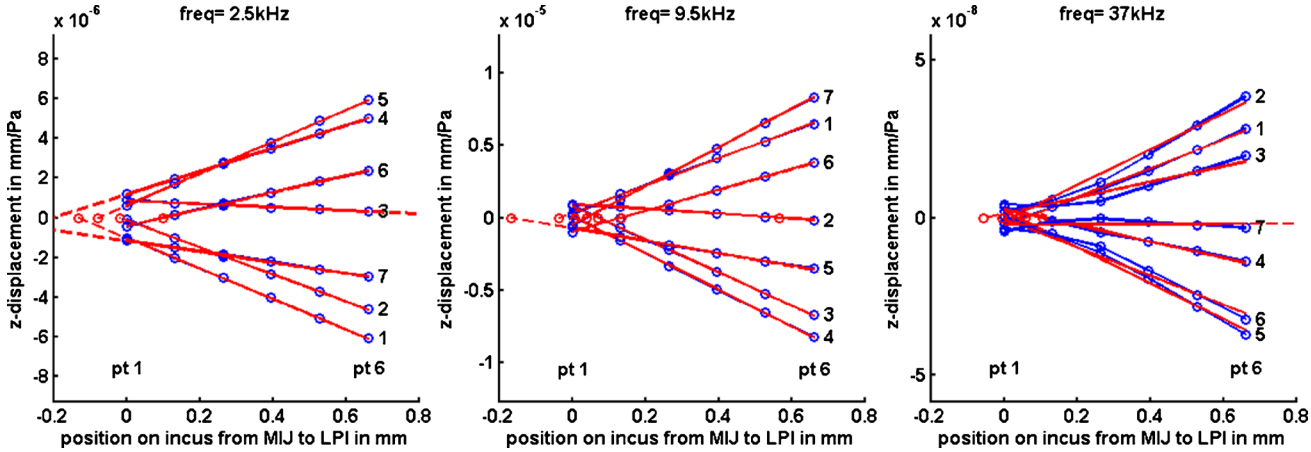

FIG. 5. Displacements of the six interpolated points on the incus between the MIJ and the LPI shown in Fig. 3 (animal 9d8) for seven equally spaced phases in a cycle (annotated one to seven) plotted as a function of position (*blue circles*); *left panel* 2.6 kHz, *middle panel* 9.5 kHz, and *right panel* 37 kHz. The change in mode of vibration is smaller than that for the malleus in Fig. 4. In *red,* a rigid-body fit to the experimental data is shown. The displacements at the "experimental points" (obtained after spatial interpolation to get collinear points) align nearly perfectly with the straight line segments of the rigid-body fit, except for the highest frequency where a small deviation from linearity in the thinnest part of the long process of the incus may indicate some bending.

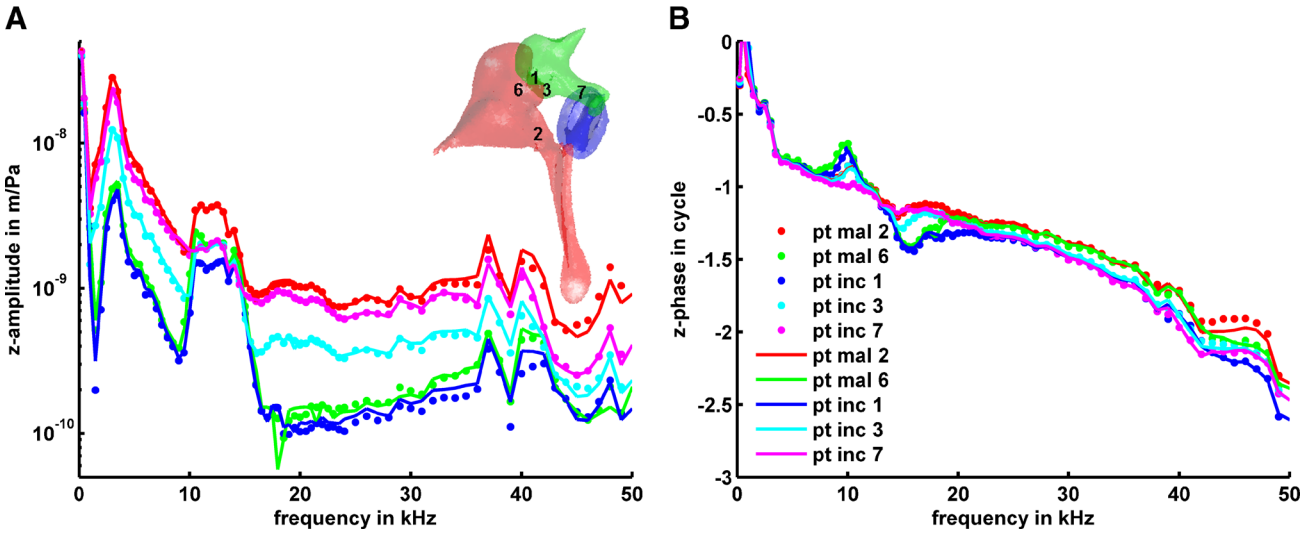

FIG. 6. The goodness of the rigid-body fit throughout the entire experimental frequency range is illustrated for animal 11d8 for two points on the malleus and three points on the incus. In **A**, the directly measured amplitudes of vibration normalized by sound pressure, and in **B** the corresponding phase relative to sound pressure for a medium range observation angle are shown as *colored dots* and the result of the rigid-body fit as *solid lines*. The *insert* shows where the observations were made on a view of the chain as seen during the experiment and the legend clarifies the color codes. Note that the fit used the observations at all observations points and angles. For all points, the agreement between experiment and fit is high up to about 30 kHz, and then some small differences are seen which could be due to the small bending seen in Figs. 4 and 5.

results of the rigid-body analysis of experiments on different animals are presented below. The 3D components are specified in the anatomical coordinate system introduced earlier (Fig. 2). Results will be presented along with an error estimation. How these were calculated is first explained.

Error Estimation

Every measurement is prone to experimental error, and this error propagates along when the data are used in subsequent calculations. To arrive at the results presented in the next section, different steps are involved; 1D vibration measurements (amplitude and phase for each probed frequency) collected with different observation angles are used simultaneously in a fitting procedure to obtain the rigid-body translation and rotation displacements for a given frequency. These displacements are then transformed into the anatomical reference frame using a coordinate transformation matrix. This matrix is obtained in two steps; first, a 3D model of the gerbil ossicular chain is registered with the positions of the experimental observation points and then the 3D model is shifted and rotated into its position in the anatomical reference frame.

To get an estimate of the errors on the experimental amplitude and phase, we calculated frequency by frequency the standard deviations (stdev) of the amplitudes and phases of a few (e.g., 4 or 5) frequency responses of repeated measurements on a given observation point, some measured in direct succession, some after intermediate measurements at other locations. For each frequency, the absolute error of the amplitude (stdev) was converted into a relative error by dividing by the amplitude. The relative errors of the amplitude and the absolute errors of the phase were more or less uniformly distributed across frequency with a few outliers (for 3 or 4 out of 75 frequencies) with up to twice the average value. The average value over frequency of the respective relative and absolute errors was taken as the experimental error of an individual observation and amounts to ~5 % for the amplitude and of 0.1 rad for the phase. In a second step, we calculated, frequency by frequency, the error on the rigid-body in-phase and out-of-phase translation and rotation displacements using standard error-propagation formulas (in a previous paper (Decraemer et al. 2007), we used a Monte Carlo technique for this, but both methods are equivalent as the rigid-body fit is essentially a multivariable linear fit). During this procedure, we neglected the error on the goniometer angle readings and on the coordinates of the observation points as they are determined with high precision, ~0.05 ° and 5–10 μm, respectively. In a third step, we calculated the error propagated onto the amplitudes and phases of the rigid-body displacements when they are expressed in the anatomical frame. As the phase angles are ultimately obtained using the arctangent function, which is highly nonlinear in the neighborhood of π, regular error propagation (which assumes that in a small interval the function can be approximated by a Taylor series

truncated after the linear terms) gives very unreliable results, and, in such cases, it is advised to use the Monte Carlo method to estimate the errors (Press et al. 1989). We produced a large number (100) of new rigid-body in- and out-of-phase displacement sets by adding frequency-by-frequency random noise drawn from a normal distribution with a mean of zero and a variance equal to 0.75 times the error on the in- and out-of-phase displacements. Each new set of data is then transformed in the anatomical frame, and the amplitude and phase are obtained. The stdev of these 100 new amplitudes and phases are calculated for each frequency and taken as the errors on the rigid-body displacements in the anatomical frame. Note that in the set of 100 "Monte Carlo" phase angles obtained by the arctangent function, jumps of 2π are present, when the undisturbed phase angle is in the neighborhood of $\pm\pi$. Before we can calculate the stdev of this set, we have to get rid of the 2π jumps; to do this automatically, a threshold was chosen, and all phase values below this threshold were raised by 2π. This procedure was repeated for a large number (here also 100) of stepwise-increasing thresholds between $-\pi$ and $+\pi$ each time the stdev of the "unstepped" phase angles was calculated. The smallest stdev thus obtained was adopted as the error on the experimental phase.

It is obvious that the final results are also influenced by the registration of the observation points and the choices made when the 3D model is brought into the anatomical frame, since adopting an intrinsic frame for a biological object is always an approximate and subjective process. We did not take this into consideration when calculating errors, but it must be kept in mind that such uncertainty is also present.

Translation Displacements of the Malleus and Incus

The anatomical frame we have chosen (Fig. 2) has the *x*-axis coinciding with the line that joins the posterior incudal tip to the anterior mallear tip, the anatomical suspension points of the ossicles. If our *x*-axis indeed played the role of a fixed-rotation axis, the rigid-body translation would be zero (or at least very small in reality) whichever point along the axis is chosen as the origin (here, the point is at the MIJ). This translation is not perfectly zero as we will see in this section, but its contribution is small with respect to the displacement due to rotation as we will see in the motion animations of Figs. 9, 10, 11, 12, 13, 14, and 15. With the choice of reference frame made [translation is dependent on the origin of the reference frame chosen (Eq. 7)], we can interpret this translation motion as a small jitter of the anatomical axis while the ossicles vibrate about it. As the malleus and incus behave as separate ossicles in the gerbil, we cannot rule out that this jitter may be different in amplitude and phase for the malleus and incus parts of the anatomical axis. Frequency responses for the three components of the translation displacement of the malleus and the incus (all expressed relative to sound pressure) are shown in Fig. 7 (thick lines) for two animals measured under anesthesia. The experimental error (calculated as described above) for the amplitude is shown by plotting a thin line corresponding to the amplitude plus the experimental error. The experimental error for the phase is shown with thin lines corresponding to the phase plus and minus the error. (Amplitude minus error is less useful because the amplitude is on a logarithmic scale.) Individual measurements are shown to illustrate similarities and dissimilarities between animals. Averaged data are not shown because averaging has a low-pass filtering effect that wipes out individual details.

Figure 7 has four major panels, each subdivided in two with the amplitude response in the upper box and the phase response in the lower box. The results for animal 11d8 are shown in the upper panels and for 16d8 in the lower panels. (The animal identification, 11 or 16, and the sort of data displayed, amplitude (-a) or phase (-p), are also reflected in the panel naming.) Results for the malleus are in the left column and for the incus in the right column.

Note that the amplitudes and phases for frequencies below 4 kHz are affected by the opening of the PF (as shown for velocities in Fig. 3 of de La Rochefoucauld et al. (2010)). We state this caveat and keep the data in the graphs as some useful information common to malleus and incus would be lost otherwise.

Figure 7, panel M11-a, shows that all three translation components have very similar trends in the amplitude-versus-frequency curves across the entire frequency range; the *y* component (green) is mostly a little larger than *x* and *z* and all curves are slightly jagged. Around 10 kHz, a small maximum is seen for all components, followed by a decrease by about a factor of five. The curves level off between 20 and 40 kHz and have a slight decreasing tendency at higher frequencies. A rather similar picture is seen for the 11d8 incus (panel I11-a); the general trend of the curves is alike, except for the *y* component, which dominates by a factor of 5 than the other components in the 4–10 kHz region. Here, also, we observe for all components a small peak at 10 kHz, now followed by a decrease by about a factor of 10 between 10 and 20 kHz, a slight increase between 20 and 40 kHz, and a slight decrease towards 50 kHz. Overall, the curves for the translational amplitudes for the malleus and incus have similar shapes and levels. For animal 16d8, results are grossly comparable with those of animal

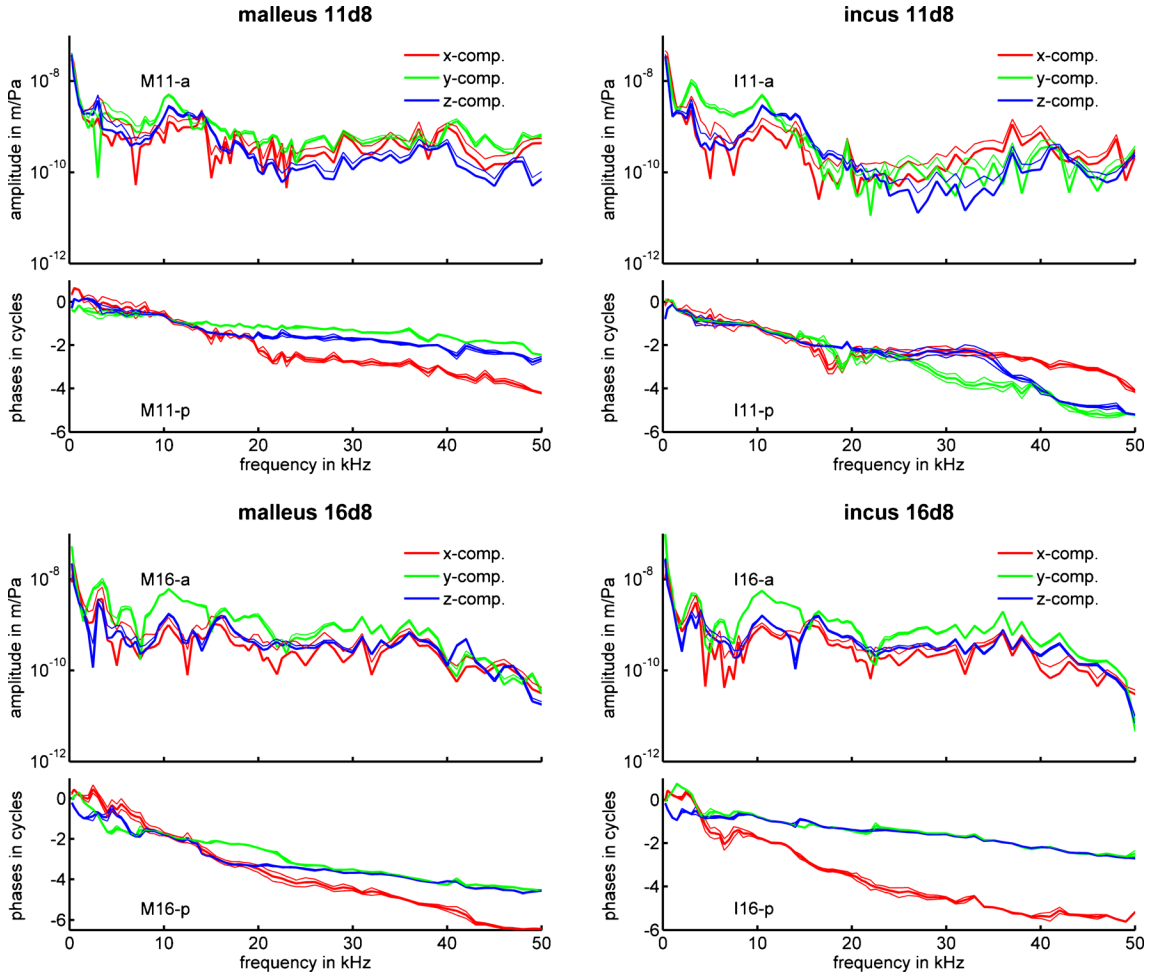

FIG. 7. Rigid-body translation displacement components as a function of frequency for the malleus and the incus of two animals in anesthetized condition are shown. In the *left column*, the malleus frequency responses (amplitude top box, phase directly below) are shown and in the *right column*, those for the incus. Panel headings indicate for which animal data are shown, and panel names whether amplitude (*-a*) or phase (*-p*) is shown. For both animals, there are trends in the amplitude and phase curves of the malleus and incus that are quite similar. Between corresponding curves of the different animals, there are similarities but also substantial inter-animal differences.

11d8, but there are some inter-individual differences: in panels M16-a and I16-a of Fig. 7, the amplitudes of the *y* components of the malleus and incus are the largest at almost all frequencies and they are very similar for the two ossicles. The other components are generally three to five times smaller up to 40 kHz, and then all three components have similar amplitudes. The *z* component is somewhat larger than the *x*-component at most frequencies.

The amplitude error curves show that the errors on the larger amplitudes are very small (<10 %, the thin lines coinciding with the thick lines). Not unexpectedly, the relative errors are somewhat larger (mostly ~10 to 20 %) on the smaller amplitudes, but because the amplitudes are small their errors have only a small effect on the vibration mode. The translation components are therefore determined with good accuracy, and irregularities of the curves are not caused by experimental error. The errors on the phases are of the order of 0.03 cycles (10 °) for the components with the largest amplitudes; for the components with smaller amplitudes, they may amount on average to values of 0.08 to 0.11 cycles (30 to 40 °), but again, variations in amplitude or phase of these small components hardly change the overall vibration mode.

Panels M11-p and I11-p in Fig. 7 show that for the malleus between 3 and 12 kHz and for the incus below 15 kHz, all components are nearly in-phase, while substantial phase differences between the components are developed at higher frequencies. For the malleus of animal 16d8 (Fig. 7, panel M16-p), the *y*- and *z*-component phases are almost the same in the 8–13 kHz region and at frequencies above 23 kHz, while the *x* phase is strongly different from the other two except in the 9–12 kHz range, where *x*, *y*, and *z*

phases are the same. For the incus (panel I16-p), the *y* and *z* are nearly the same above 5 kHz, while the *x* component is different from the *y* and *z*, and acquired a phase lag about twice that of the other two at 50 kHz. A common trend is that the phase decreases with frequency; some components display here a rather linear trend above 5 to 10 kHz, but other components do not.

Above 4 kHz, the amplitudes of the three translation components are all of the order of 10^{-9} m/Pa, which is also the magnitude of the directly measured vibrations (almost along the *z*-axis) at the points on the malleus and incus with the smallest displacements, that is, the points near the MIJ such as points M6 and I1 in Fig. 6A. This can be seen as a check on the calculated translation displacements.

Overall, we can conclude that there is a small, frequency-dependent global translation of the ossicles that differs in amplitude and phase between different animal and that hence the rotational axis does not remain fixed during the cycle. In addition, Figs. 4, 5, and 6 show that the closer we got to the anatomical axis, the smaller the measured amplitude of vibration became, indicating that, besides the global translation of the malleus and incus, a rotation about an axis in this neighborhood must be taking place. This rotation is analyzed in depth in the following section.

Rotation Displacements of the Malleus and Incus

From an anatomical viewpoint, the malleus and incus seem to be configured to rotate about the anatomical axis defined by their anchoring points in the middle-ear cavity (our *x*-axis). Let us see to what extent this was true. In Fig. 8, with a layout similar to that of Fig. 7, rotational components for the malleus and incus are displayed.

Considering all four panels of Fig. 8, it is striking that the errors on the rotation amplitudes are very small when the amplitudes are large: the thick and thin lines, showing amplitude and amplitude plus error respectively, coincide. For the smaller amplitudes, blue and green in I11-a and M16-a, the thin amplitude-plus-error line is visually different from the thick data line with differences amounting to an error of approximately 20 to 30 %. These errors on the small components are not really problematic as the large components are preponderant. The phase panels show that rotation phase errors are small so that we can conclude that the rotation mode was determined with good precision.

The rotation component about the anatomical axis, red line in all amplitude panels in Fig. 8 (M11-a, M16-a, I11-a, and I16-a), dominates the other components at most frequencies up to 35 kHz; the other components become of equal magnitude in certain small frequency intervals, and consistently above 35 kHz. For both animals, the rotation components about the anatomical axis are almost exactly the same for the malleus and the incus. They are also very similar for the two animals. For the other components, there are substantial differences between the malleus and the incus and between the two animals. The phases for the anatomical axis components (red lines in all the phase panels) are also very similar and present as more or less smoothly decreasing curves with frequency. In the phase curves for the other components, some one-cycle phase differences which could be due to differences in the phase unwrapping are present. (Note that when showing the motion of the ossicles as an animation this has no influence.) In both animals, there are substantial phase differences between the *x*-axis component and the other two components for both malleus and incus, and the phases of the *y* and *z* components are also different between the two animals. A more in-depth analysis of the differences in amplitude and phase of this component will be made in the section "Malleus and Incus Rotation about the Anatomical Axis.". The other components, which cause the true rotation axis to wobble about the anatomically defined axis, are somewhat different for malleus and incus, and in different animals.

MODE OF VIBRATION OF THE MALLEUS AND INCUS

For the description of the translation and rotation components in the previous section, we had to choose a reference system a priori, but we found that rotation components about the axes perpendicular to the anatomical axis (*y* and *z*) were also important, indicating that the rotation axis did not correspond to the anatomical axis. When using the screw axis concept, no a priori choice for the rotation axis is required: the aim of the method is to determine the rotation axis from the motion itself. A 3D plot of the positions of the ossicles and their instantaneous rotation axes at a number of phases during the vibratory cycle can nicely illustrate the mode of ossicular vibration. Note that we continue to use the anatomical frame to make these 3D plots, which allows one to relate the instantaneous rotation axes to the anatomical axis. Such animation plots have to be made frequency by frequency, and covering the entire experimental frequency range would require too many figures. In the present context, we will select a few frequencies where typical vibration modes are seen. On the websites of two of the authors (http://audilab.bme.mcgill.ca/ossmot/ and https://www.uantwerpen.be/en/rg/bimef/downloads/ossicular-motion/), we have made available "apps" (requiring a freely distributed MATLAB Runtime

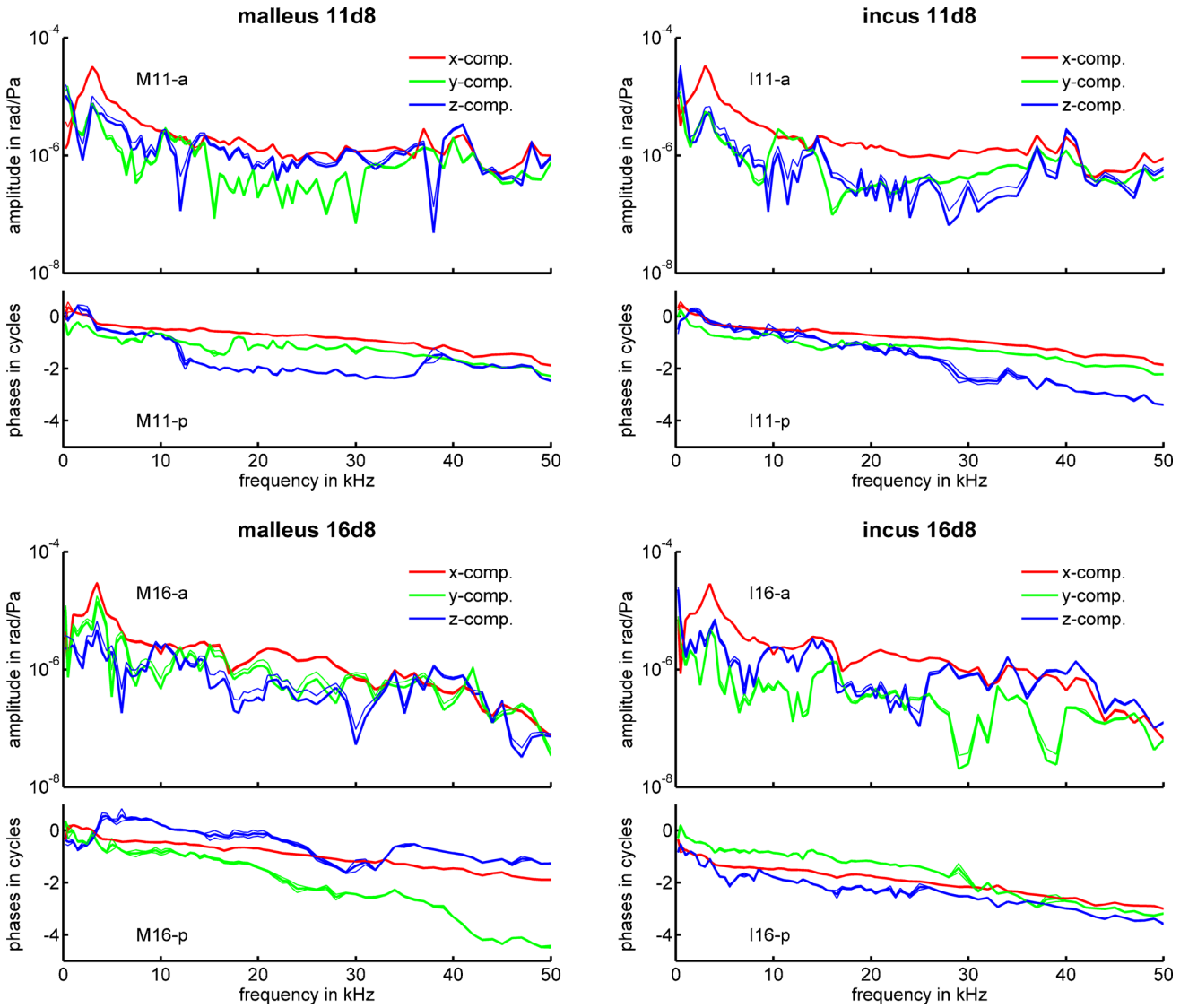

FIG. 8. Rigid-body rotation displacement components as a function of frequency for the malleus and the incus of two animals are shown: in the *left column*, the frequency responses for the malleus (amplitude top box, phase directly below), and in *the right column* corresponding incus data. Panel headings indicate for which animal data are shown, and panel names whether amplitude (-*a*) or phase (-p) is shown. Most striking is that the *x* component of the angular amplitudes for the malleus and incus are almost identical up to 40 kHz, and then there are small differences. This component shows also the same trend for the two animals. Rotation phases for the *x* components of malleus and incus are also very similar.

Component, MRC) that permit viewing of animations of the malleus and incus motions for all frequencies. Various parameters can be set, such as the frequency, the viewing angle, the inclusion of the screw axes for malleus and/or incus, and optional output to AVI movie files. Information on how to install the MCR and run the app is included on the websites.

Introduction to the Layout of the Plots Showing the 3D Motion of Malleus and Incus

In the next section, the 3D periodic motions of the malleus and incus will be graphically shown for a set of frequencies with typical vibration modes. A lot of information will be embedded in these figures and to familiarize the reader with them we explain their layout in Fig. 9. Note that we selected for the present figure a frequency of 9.5 kHz (animal 11d8) not because the mode is most typical but because the motion allows us to introduce many features that may be present in the following plots for different frequencies. The motions of the malleus and incus are illustrated as animations, projected onto the *x*, *y* plane in Fig. 9A, and onto the *x*, *z* plane in Fig. 9B, by showing their positions at seven equally spaced phases (t=0, T/7, 2T/7, …, 6T/7) in the cycle, as if it were a stroboscopically illuminated scene. The choice of seven phases is a compromise; it is sufficient to

document the motion during the entire cycle without overloading the figures; note that seven phases were preferred over six because the use of six produces overlapping (or nearly overlapping) positions for displacement phase angles that are equal to (or close to) a multiple of $\pi/6$. The rest positions of the malleus and incus are also shown using transparent black and can be discerned amidst the other vibratory positions shown in transparent red for the malleus and green for the incus. It is inevitable that the other seven positions obscure the rest position in certain views. For the sake of orientation, the rest position of the stapes is also shown (in gray), although no measurements on the stapes were done during the present experiments. Using motion parameters for the stapes measured earlier on other animals (Decraemer et al. 2007) to present also the motion of the stapes in the present plots was unsatisfactory; we could find a dataset for the stapes that matched the present malleus and incus motion at some but not at all frequencies. In a separate section "Complete Ossicular Motion," we will show an animation that includes the three ossicles for a low frequency.

Vibratory displacements are so small compared with the size of the ossicles (10^{-8} m or smaller) that they had to be scaled up to make them visible. The scaling factors that we used were automatically calculated so as to scale the maximal displacement for each frequency to the same fraction (0.2) of the stapes height (1.2 mm) and therefore varied with frequency; scaling factors (displ. scal) and stimulus frequency will be given in the overall figure titles of Figs. 10, 11, 12, 13, 14, and 15. For Fig. 9, the displ. scal was 52,000.

In all panels, the rest position of the anatomical axis, the *x*-axis, is shown as the horizontal dot-dashed black line. For three landmark points (the tip of the manubrium, the AMP and the PIP), the displacement paths during the cycle were calculated using the rigid-body displacements. These paths were plotted in black centered on the corresponding landmark rest positions in Fig. 9A, B. It can best be seen at the tip of the malleus that these paths are ellipses in 3D space. The positions of the manubrium tip for the seven time instants during the cycle are shown as black dots on the path of the umbo, annotated 1 to 7. A most striking feature is the non-negligible motion of the AMP and the PIP, which indicates that the anatomical axis is not stationary during the cycle but wobbles. Note that structures at the supporting points of the malleus and the incus (AMP and PIP) must be sufficiently flexible to allow these very small motions at the attachment points. In the *x*, *y* projection of Fig. 9A, the lenticular process of the incus is seen to have a motion component parallel to the surface of the stapes head. In Fig. 9B, the same 9.5 kHz motion is viewed along the *y*-axis. The sequential positions of the malleus during the cycle indicate that it performs a rotary motion in combination with an up-and-down translation; while the PIP is nearly stationary in this view, the AMP moves up and down in the *z* direction.

In Fig. 9C–F, we analyze some of the features of the screw axis for this 9.5 kHz motion. To simplify the figure, no vibration positions are shown, only the rest positions of malleus, incus, and stapes for orientation purposes. In Fig. 9C, D, the screw axis of the malleus is shown for the seven time instants with the same viewing directions of the animations in Fig. 9A, B, respectively. The rotation vector is drawn as a solid dark red line (labeled 1 to 7) originating from the point R_0 (marked with a magenta dot) which is the point on the screw axis closest to the origin of the anatomical reference frame (marked with a black circle). The rotation vectors are drawn with lengths that are proportional to their magnitudes by multiplying them by a scale factor that is equal to 1.2 times the stapes height (1.2×1.2 mm) divided by the magnitude of the rotation vector with maximal length. This scale factor also differs from frequency to frequency; its value is not relevant for the evaluation of the modes of vibration and for simplicity it is not mentioned further. Since R_0 is the point on the axis that is closest to the origin, the line from R_0 to the origin is normal to the axis, and drawing this extra line (dashed magenta) makes it easier to imagine the spatial orientation of the screw axis knowing that the 3D angle between the screw axis and the dashed line is always a right angle. It helps us to picture the differences in spatial orientation of the screw axes, which in the example of Fig. 9C, D all have different spatial directions. We have drawn similar plots with the screw axes of the incus in Fig. 9E, F (again same views of panels A and B of Fig. 9, respectively). The line types were kept the same but now the rotation vectors are shown in dark green, while the magenta construction lines and dots are now in cyan.

In principle, we can draw the rotation vector $\boldsymbol{\omega}$ at any point along the rotation axis; it does not indeed make any difference as it just represents the rotation about the axis. Using the point R_0 as anchor point has some advantages. When we follow the point R_0 during a cycle, we see that it travels the same ellipse twice. This is because for a harmonic motion the rotation and translation vectors, $\boldsymbol{\omega}$ and $\mathbf{v}_{trans}$, have the same orientation and magnitude twice in a cycle, but with opposite directions, for points T/2 apart. As a consequence, R_0 must be the same at any two points that are T/2 apart. Note that for a fixed axis, the ellipse would shrink to a point and $\boldsymbol{\omega}(t)$ would oscillate harmonically about this point along the axis fixed direction. For the sake of drawing the elliptical trajectory of R_0 as a smooth curve, 400 phases were

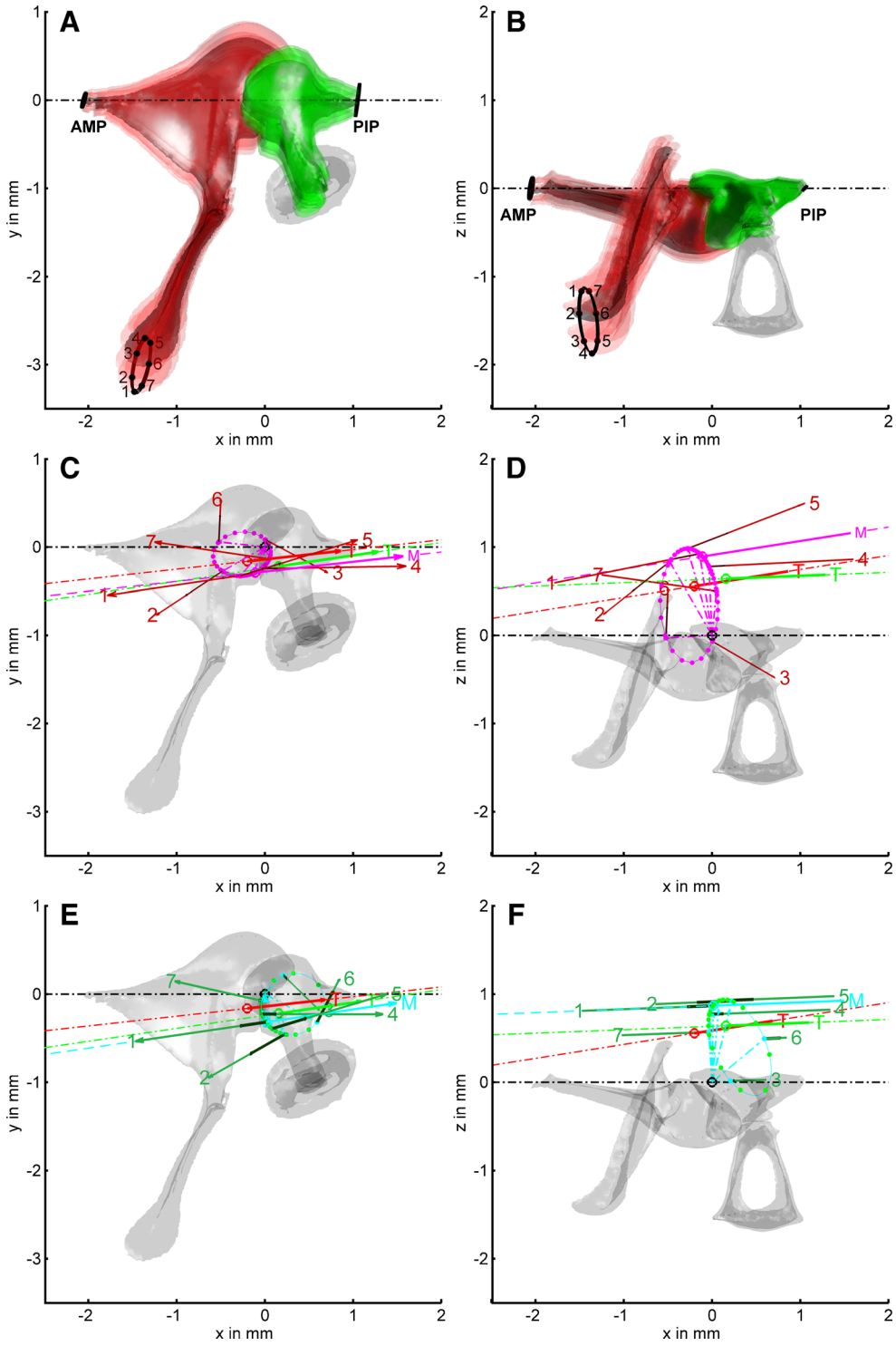

used. The positions of R_0 at 40 equally spaced time instants were marked on the ellipse with bright red dots. (Only 20 dots are seen as the points of the second half cycle fall on top of those of the first half cycle.) Because the phases used are equally spaced in time, the screw axis flips quickly through the part of the ellipse with widely spaced points and spends most of the time of the cycle where the points are clustered.

The screw axis with the maximal rotation amplitude (*maximum rotation axis*, MRA) is shown as a thick magenta line for the malleus in Fig. 9C, D and as a thick cyan line for the incus in Fig. 9E, F, extended in both directions as dashed lines with labels *M* in the corresponding colors. When we look at the spacing between the R_0 points around the ellipse, we see that the MRA is at the point of the trajectory where the speed of R_0 along the trajectory is lowest.

FIG. 9. In **A** and **B**, the 3D motion of the malleus (*red*) and incus (*green*) is shown at seven equally spaced instants of time in the cycle (t=0, T/7, T/7...6T/7). The stapes (*gray*) is only included as reference and is shown as stationary. The rest position of the anatomical axis (the *x*-axis) is shown in all panels as the *horizontal, black dot-dashed line*. For the U, the AMP and the PIP, the displacement paths during the cycle are plotted in black in **A** and **B**. The path of the U illustrates best that these paths are generally ellipses in 3D space. The positions of the U for the seven time instants during the cycle are shown as *black dots* on the path of the umbo and annotated one to seven. In **A.** we look along the stapes piston direction (along our *z*-axis), in **B** along the *y*-axis (the projection plane is annotated in each panel). In the *middle panels* **C** and **D**, the instantaneous rotation axis (screw axis) of the malleus is plotted in relation to the stationary ossicular chain; the same viewing angles are used as in the upper panels. *Solid magenta lines* illustrate the instantaneous rotation vectors originating from the points R_0 (shown as *magenta dots*), and annotated one to seven at their endpoints. *Dashed magenta lines* connect the origin of the coordinate system (*black circle*) to the points R_0 which are the points on the instantaneous rotation axes closest in 3D to the origin. During the cycle, the point R_0 travels around the magenta ellipse. Positions of R_0 at 40 instants that are equidistant in time, plotted as *bright red dots* on this ellipse, indicate where the rotation axis spends most of the time during the cycle. The instantaneous rotation axis with maximal length is shown as the *thicker solid magenta vector* annotated with *M* and extended at both ends with a *dashed magenta line*. The mean position of R_0 during a cycle is shown as the *red open circle inside the ellipse*; here, the time average rotation vector in half a cycle (T) has its origin (*thick red line* extended in both directions with a *dot-dashed red line*; for the incus, the TARA is similarly shown but in *green*). The *dark red sleeves around the instantaneous axes* show the slide displacement about the instantaneous rotation axis. Displacements and slide vectors are all scaled to be shown as a fraction of the stapes length with scale factors mentioned in the figure title. In **E** and **F**, a similar layout is used for the screw axes of the incus, while *red* is replaced by *green* and *magenta* by *cyan*. For easier comparison of the positions of the TARAs and MRAs of the malleus and the incus, the TARA of the incus is also shown on the figures with the screw axes of the malleus and vice versa using the same color code.

The average position of R_0 during a cycle was calculated for the malleus (open bright red circle in Fig. 9C, D) and for the incus (open bright green circle in Fig. 9E, F). The average value of the rotation vectors was also calculated but in the range of a half cycle between rotation vector amplitude minima (a quarter cycle before and a quarter cycle past the instant of time corresponding to the MRA). A calculation based on 400 time points in the cycle was used here. (Taking the average over the whole cycle would yield zero.) Such a *time-average rotation axis* (TARA) can be seen as some kind of *effective* rotation axis during the cycle. The TARA for the malleus is shown as the thick bright red line starting at the red open circle and extended in both directions as a dot-dashed line of the same color to accentuate its direction, and for the incus as the thick bright green line also extended with dashed dotted line of the same color at both ends, with labels *T* in the corresponding colors. Because we calculated the TARA in a symmetric interval around the MRA its direction corresponds to that of the MRA. (In the "Appendix," we prove that for the chosen symmetric interval of $\pm\pi/2$, TARA=$(2/\pi)$ MRA, indicating that the vectors are parallel.) The position of the time-averaged R_0, which, as the average of points on the ellipse must lay somewhere inside the ellipse, differs from that of the R_0 of the MRA, a point on the ellipse. Both MRA and TARA axes give an idea of the major rotations during the cycle. To set up a link between the plots with the malleus and the incus screw axes, the TARAs of both the malleus and incus were plotted in both the panels with the malleus screw axes (Fig. 9C, D) and the panels with the incus screw axes (Fig. 9E, F).

The screw axis concept also involves the slide velocity, the global displacement of the rigid body along the instantaneous rotation axis. In Fig. 9C, D, we have drawn the slide velocities for the malleus at the seven instants of time as deep dark red sleeves surrounding the screw axes and originating also from the points R_0. Similarly, the slide velocities for the incus were drawn in Fig. 9E, F as deep dark green sleeves. The scaling factor (slide-scal) used here is expressed as a multiple of the displacement scaling factor. In Fig. 9C–F, slide-scal=6.9×disp-scal, indicating that the slide displacements are about seven times smaller than the maximal total displacement (rotation and translation) of the entire malleus and incus. In the same figure, we see how the slide varies in magnitude and direction during the cycle. Dividing visually the lengths of the dark red lines by seven and comparing them with the displacement components of the malleus in Fig. 9A in the same direction as the slide vectors, we see indeed that even for this small value of slide-scal (one of the smallest throughout the frequency range) the slide does result in only a small displacement. The maximum slide values sometimes occur at times of small rotation so that sliding then dominates the displacement. At most frequencies, the slide-scal factor is more than 50 to 100 times the disp-scal factor and in those cases we may directly conclude that slide displacements are negligible compared with the rotation displacements.

The individual screw axes of the malleus and incus change with time in very similar ways as can be seen comparing panels C and E and panels D and F in Fig. 9. As a result, the TARAs of malleus and incus are also very much alike. In the view along the *z*-axis of Fig. 9C, E, the TARAs for the malleus and incus are tilted with respect to the *x*-axis, that is the anatomical axis. In Fig. 9D, F, we see that both TARAs run at a distance of about 1 mm lateral to the anatomical axis but slightly tilted with respect to it. (Side note: the MATLAB command quiver3 was used to plot the screw axes and slide vectors; depending on the angle that the vectors make with the *z*-axis, the arrowheads

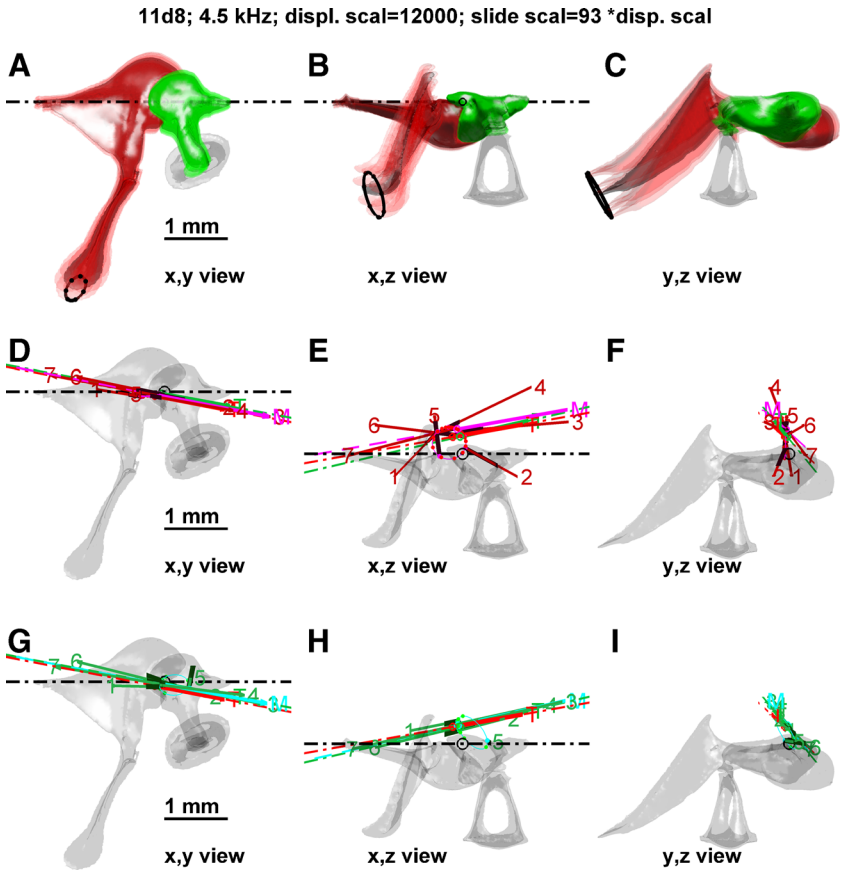

FIG. 10. Vibration mode of animal 11d8 at a low frequency of 4.5 kHz displayed in the fashion introduced in Fig. 9, but now views along all three coordinate axes are shown by adding a third column to the right with views along the *x*-axis. The animal identification, the frequency, and the scaling factors for the displacements are annotated at the top. The *top row* has the motion animation, the *middle row* has the screw axes for the malleus, and the *bottom row* has the screw axes for the incus. For this relatively low frequency, the rotation of the malleus takes place about an axis that is running slightly laterally to the malleus and incus block (*x, z* view *middle panel*). The MRA makes an angle of about 10 ° with the anatomical axis (*x*-axis, shown as the *black dashed-dotted line*) in the *x, y* plane (**D** and **G**), and makes about the same angle with the *x*-axis in the *x, z* plane (**E** and **H**). Note that the screw axes for malleus and incus are fairly well aligned at each phase of the motion.

show up (as in Fig. 9C) or disappear (as in Fig. 9D). We did not try to solve this problem because, while helpful when visible, the arrowheads are not really necessary since we clearly mark the origin of each vector and annotate the end points with the phase sequence number.) We see also that in the *z* view (Fig. 9C, E), the projections of the TARAs of the malleus and the incus are almost parallel (~1 ° apart); since in Fig. 9D, F the angle between the axes is also small (~5 °), this means again that at this frequency the rotations of the two ossicles occur about nearly the same immediate rotation axes (as was already observed above).

Vibration Mode as a Function of Frequency

We are now ready to present 3D malleus and incus motion at a few frequencies in selected ears to illustrate several typical vibration modes. For each frequency plots similar to Fig. 9A–F will be used, but we have added at the right an extra column showing the views along the *x*-axis; the three panels (ABC) in the top row show the animations of the ossicles, the panels of the middle row show the screw axes for the malleus (DEF), and the bottom row the screw axes for the incus (GHI). To simplify the figures in panels A, B, and C the ellipses at the AMP and PIP and the annotations at the *U* are left out to simplify the figures, and in panels D–I he position vectors R_0 are not drawn to diminish clutter. For easy comparison with the TARA location, the anatomical axis (*x*-axis) is added to each panel as a black dashed dotted line. Each view shows interesting aspects of the motion and we must combine views from all three directions to grasp the nature of the mode. Note that it is inevitable that in certain views parts of the malleus or incus and some screw axes and their annotations hide one another; using different views and, even better, magnifying the electronic version of the on-line paper can greatly help the readability of the plots. The

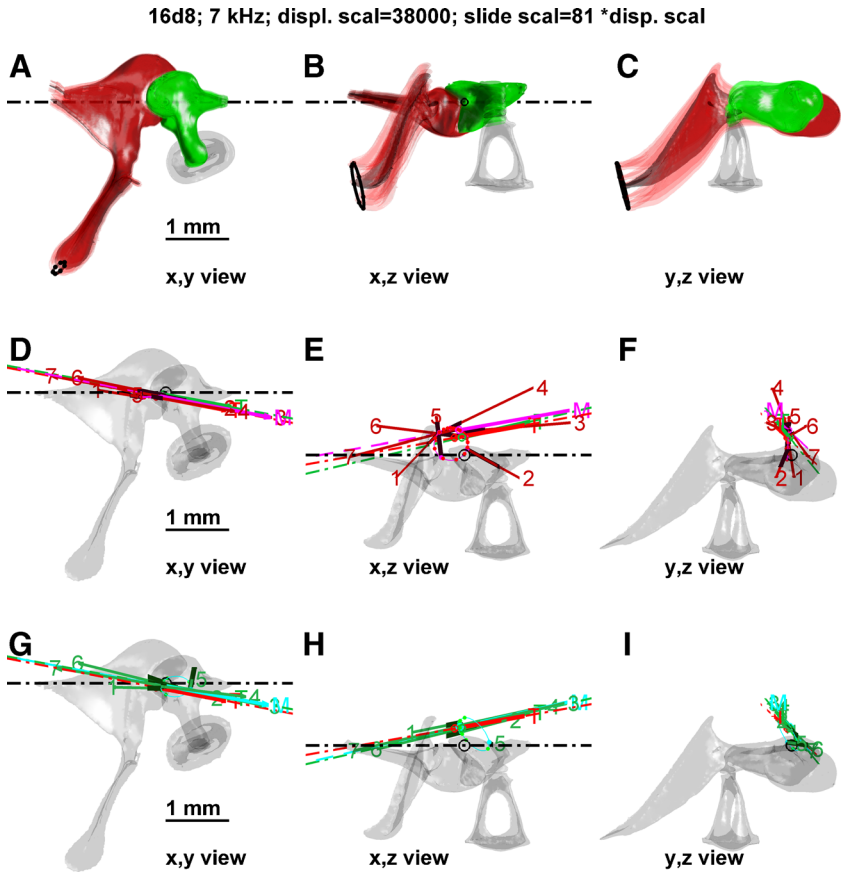

FIG. 11. Vibration mode for animal 16d8 at a frequency of 7 kHz (displayed as in Fig. 10).

position of the origin (and hence the *x*-axis) is because of the overlaying of the different plots of the malleus and incus for each displaced position, invisible in panel C, but it can easily be tracked down in panels G and I just below, which use the same view. Although we will discuss the characteristics of the screw axis for each case, the direct visual observation of the "stroboscopic" ossicular chain in the three orthogonal views is not only very intuitive but also often very instructive.

From 1.5 kHz on, the mode remains quite the same up to about 9 kHz. The mode at 4.5 kHz is illustrated in Fig. 10. In Fig. 10C, we have a posterior to anterior view and we see the manubrium clearly rotate in the *y*, *z* plane; the motion of the umbo is reduced in amplitude by about four times at the LPI, which has an up-and-down motion in the stapes piston direction and also a component of similar magnitude parallel to the surface of the stapes head, which hints at a rocking motion of the stapes around the long axis of the footplate. Such rocking, which was already reported in cat (Decraemer and Khanna 1999), was also observed in gerbil as will be shown below (section "Complete Ossicular Motion"). Translational displacements are negligible compared with rotational displacements as we have a slide-scal of 93. The panels D and E and G and H of Fig. 10 illustrate best the location of the rotation axis: in the view of Fig. 10 panels D and G the screw axes for the malleus and for the incus are at all times nearly aligned, so as a consequence the directions of the TARAs of the malleus and incus are almost exactly the same. In the *x*, *z* projection, all screw axes for the incus are also nearly aligned (Fig. 10H), but for the malleus (Fig. 10E) the screw axis varies over the cycle (this is also apparent in Fig. 10F); nevertheless, the TARAs for the malleus and incus nearly coincided with each other. Furthermore, for both the malleus and incus, the TARA coincided almost perfectly with the MRA. All this indicates that the incus motion is a rotation about a fixed rotation axis which makes an angle of about 20 ° with the anatomical axis in the *x*, *y* plane (Fig. 10G) and runs slightly lateral to it at an angle of about 20 ° in the *x*, *z* plane (Fig. 10H). For the malleus, the rotation axis wobbles slightly around the fixed incus axis. We may conclude that the results at 4.5 kHz come close to the mode of vibration classically described as a vibration about a fixed axis going through the anchor points of the malleus and incus.

Similar vibration modes but with somewhat more variable screw axis positions, and TARAs for malleus

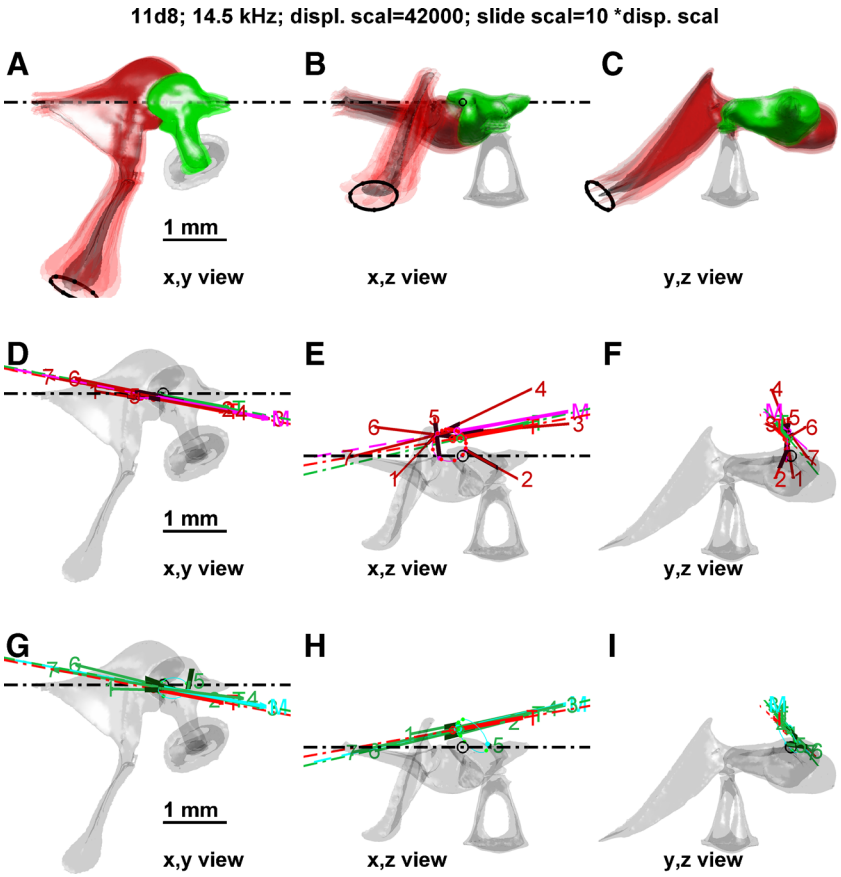

FIG. 12. Vibration mode for animal 11d8 at a frequency of 14.5 kHz (displayed as in Fig. 10).

and incus that are less perfectly aligned with each other, are seen up to 8.5 kHz in this animal.

The vibration modes at frequencies below 9 kHz of other animals are rather similar to, although less "classical" than that of animal 11d8 in Fig. 10. In Fig. 11, the vibration mode for animal 16d8 at a frequency of 7 kHz is presented. In Fig. 11C, the malleus and incus are seen to have a predominantly rotary motion in the *y*, *z* plane; in the view along *z* (Fig. 11D, G) the TARA of the incus is nearly along the anatomical rotation axis but that of the malleus makes an angle of about 20 ° with it. The two axes do not intersect in one point, but in the *x*, *y* projection of panels Fig. 11D, G the axes cross close to the MIJ. In the animation panel with the same view (Fig. 11A), we see that the anterior mallear tip has a considerable motion in the inferior-superior (*y*) direction. In the view of panels Fig. 11E, H the TARA of the incus runs slightly medial to the ligament axis at the posterior end, making an angle of about 5 ° with it. Views of F and I in Fig. 11 look almost head-on onto the rotation axes, which confirm that they are rather close to the *x*-axis. Because of the angle between the TARAs of the malleus and the incus, there will be some relative motion between malleus and incus at the MIJ.

In the frequency region between 9.5 and 15 kHz, the mode changes dramatically. Data at 9.5 kHz were presented in Fig. 9; Fig. 9C, D showed that the malleus screw axis changed strongly in direction during the cycle. The incus axis also wobbled in the *x*, *y* view (Fig. 9E), but in the *x*, *z* view (Fig. 9F), all of the incus axes are close to parallel but shifted with respect to one another. The incus TARA makes an angle of about 5 ° with the malleus TARA. The TARAs of malleus and incus have rotated counter-clockwise in the *x*, *y* view (Fig. 9C, E) relative to the axis shown in Fig. 10D, G, and have moved to a more lateral position (*x*, *z* views of Fig. 9D, F compared with Fig. 10E, H).

We show the mode for animal 11d8 at 14.5 kHz in Fig. 12. Screw axis directions now vary strongly within the cycle and the TARAs for both malleus and incus are in positions completely different from the anatomical axis in the three different views (Fig. 12D–I). The TARAs and MRAs have different spatial locations. Figure 12A–C reveal that the anterior mallear tip and to a smaller degree also the posterior incudal process move at their attachments and that the manubrium tip describes an ellipse in space with larger in-plane than out-of plane excursions. The TARAs of malleus and incus

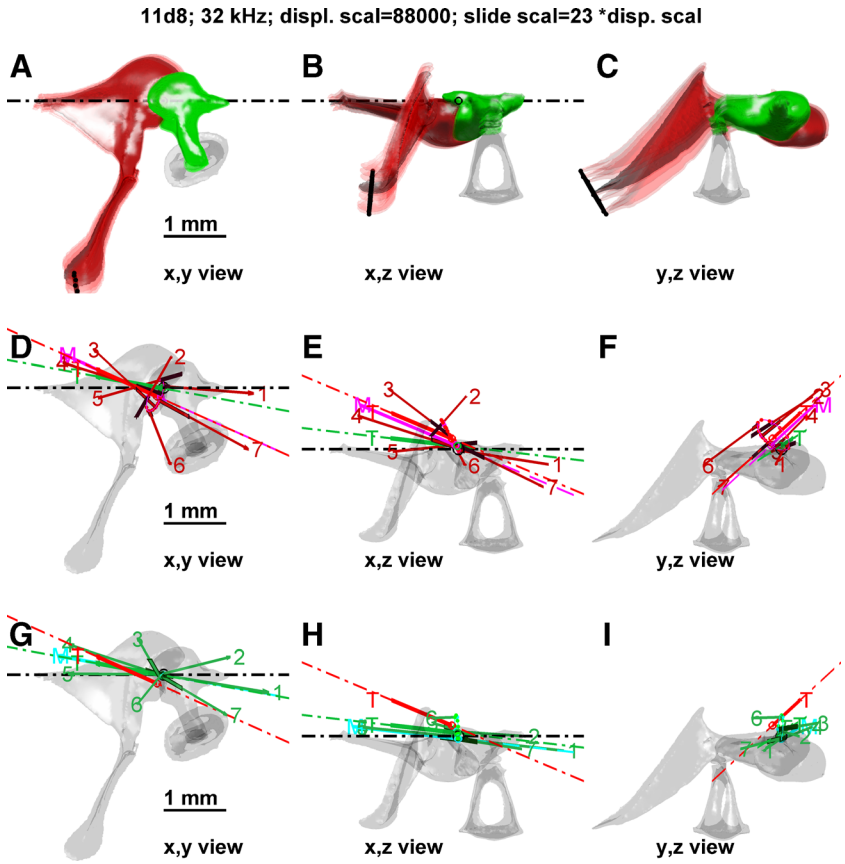

FIG. 13. Vibration mode for animal 11d8 at a frequency of 32 kHz (displayed as in Fig. 10).

describing such motions make large angles with the anatomical axis, about 45 ° in the *x*, *y* view and about 70 ° in the *x*, *z* view.

Above 15 kHz, the mode continues to change with frequency; screw axis directions continue to vary a lot within the cycle. We show an example at 32 kHz for animal 11d8 in Fig. 13. The TARA of the incus is again closer to the anatomical axis in both direction and position. Most remarkable is the change in orientation of the TARAs of malleus and incus, as if in the *x*, *y* view (Fig. 12D, G) they were flipped left to right with respect to the configuration at 14.5 kHz. The malleus and incus TARAs cross each other just medially to the MIJ, making an angle of about 20 °.

With a last example for animal 11d8 at 42 kHz (Fig. 14), we again observe a vibration mode that deviates from the classical fixed-axis rotation model. The TARAs of malleus and incus have rotated again into a position where they make large angles (30 ° to 45 °) with the anatomical axis in the *x*, *y* (Fig. 14D, G) and the *x*, *z* views (Fig. 14E, H) and this results again in in-plane displacements of the manubrium comparable to the out-of-plane displacements. TARAs for malleus and incus are not aligned with each other and their *x*, *y* and *x*, *z* projections do not intersect in the neighborhood of the MIJ.

Living Versus Post-Mortem

There was no prominent difference between vibration modes in the living animals and in the animals measured a few hours post mortem or 1-day post mortem. (A more in-depth analysis in the "DISCUSSION" section will show some small but interesting trends with time.) Figure 15 shows the vibration mode at 5 kHz of animal 9d8 that died during preparatory surgery around 10:10 am; the experimental data used for the figure were collected about 5 h later. Until 12:35 p.m. the PF opening was closed using a small piece of Saran™ wrap, but due to condensation it was removed.

Although the angle of MRA and TARA with the *x*-axis is opposite to that in Fig. 11, we see a mode that is similar to that of animal 16d8 in the same frequency range (7 kHz; Fig. 11): a rotation of the malleus and incus about a nearly fixed axis with the screw axes at most time instants aligned along the TARAs for the respective ossicles. In the *x*, *y* view of the Fig. 15D, G, the TARA for the incus is almost coincident with the

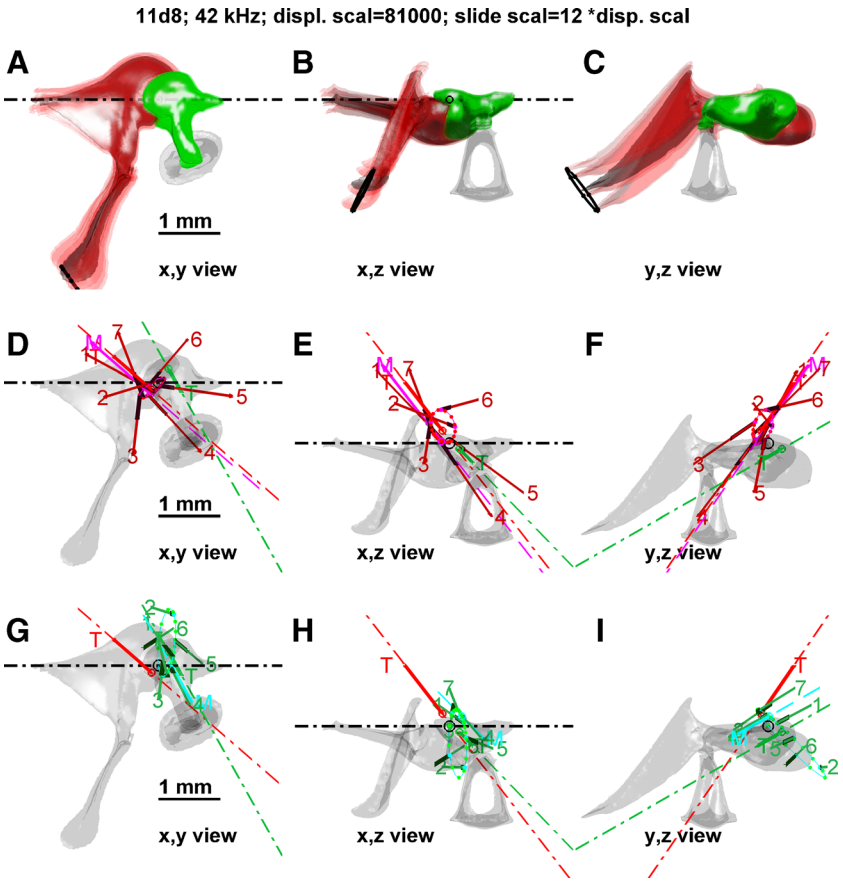

FIG. 14. Vibration mode for animal 11d8 at a frequency of 42 kHz (displayed as in Fig. 10).

anatomical axis while the TARA for the malleus makes an angle of ~15 ° with the anatomical axis. Both axes cross at about the MIJ. The *x*, *z* view (Fig. 15E, H) confirms that the incudal TARA coincides with the anatomical axis. The six panels, D–I in Fig. 15, document well the spatial direction of the malleus and incus TARA**s**.

Almost the same location of the TARA of the incus is seen up to 11 kHz; the malleus also has a nearly fixed screw axis in this frequency range, but the angle with the anatomical axis varies within about ±15 ° from the situation in Fig. 15. In the frequency range up to 11 kHz in this ear, the screw axes for the malleus and incus having a nearly fixed direction and vibrate during the cycle back and forth along the directions of the respective TARAs. At a few frequencies, the TARAs of malleus and incus are nearly coincident, indicating a very classical vibration mode. We may not readily conclude that this was typical for the PM condition as this was not seen in a second animal measured post mortem nor in measurements we performed earlier on fresh cat cadavers (Decraemer and Khanna 1999). It must rather be considered as an example of large inter-animal variability that was observed in all species measured so far. In all other frequency ranges, the classical picture was not valid even for this animal.

Malleus and Incus Displacement Amplitude and Ossicular Lever Ratios

The classical view of middle-ear motion is that of a rotation of the ossicles as a rigid block about the anatomical axis. In this hypothesis, the umbo should have only a displacement component perpendicular to the manubrium surface and the ratio of its displacement to the footplate amplitude should be equal to the ratio of the lever arms, the perpendicular distances of the umbo and footplate center to the anatomical axis ("the middle-ear lever ratio"). Despite the facts that we have shown in the previous section that the mode of vibration of the malleus and incus in the gerbil varies strongly with frequency—the classical fixed-axis rotation model of the ossicular motion is at best only approximately valid in the relatively low frequency range below 10 kHz—it is interesting to find out how the presence of rotation components perpendicular to the anatomical axis affects the displacement amplitude ratio of the umbo and the LPI.

Let us first look at two examples for the live animals, gerbils 11d8 and 16d8. Using the translation and

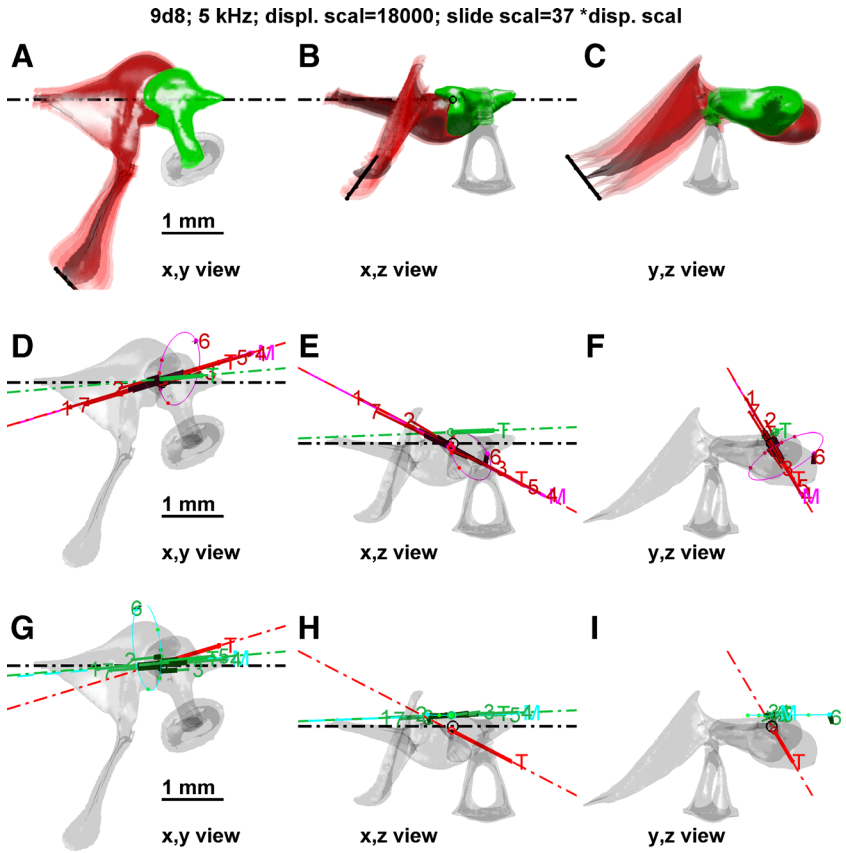

FIG. 15. Vibration mode for animal 9d8 in fresh cadaver condition at a frequency of 5 kHz (displayed as in Fig. 10).

rotation displacements obtained by the rigid-body fit, displacement responses expressed in the anatomical frame (Fig. 2) were calculated for points on the malleus at the umbo, LPM and neck of the malleus (NM), and on the incus at the LPI. Note that, even though no measurements were done at the umbo, we could calculate its response with the assumption that the manubrium is rigid. (This is only approximately true; de La Rochefoucauld and Olson (2010) found substantial bending at the manubrium tip at 25 kHz and up.) A common experimental situation is that displacement is measured along one fixed direction. Let us mimic this situation and compare the ratio of the z components of the fitted rigid-body model displacements with the anatomical lever-arm ratios. The lever arms responsible for these z displacements are the perpendicular distances to the presumed rotation axis (the x-axis), that is, the y coordinates of the respective points (umbo, LPM…). In Fig. 16A, the ratios of the z displacement amplitude of the umbo, LPM, and NM relative to the displacement amplitude at the LPI as functions of frequency are shown; the lighter colors of red, green, and blue are used for the 11d8 animal, and the darker versions are used for the 16d8 animal (see also legend). The ratios of the anatomical lever arms are added as a straight horizontal line for each "observation" point.

The deliberate choice was made to relate the three malleus displacements to the LPI displacement, contrary to the common practice of relating output (LPI) to input (say umbo, LPM, or NM) because the LPI (as its piston displacement is almost exactly equal to that of the footplate center; Decraemer et al. 2007) is probably the most meaningful displacement in the middle ear since it determines cochlear input and hence deserves to be the reference. In the range up to 10 kHz, the average z displacement ratios for the three points of 11d8 are a factor 1.2 to 1.3 larger than the lever arm ratios. Between 9 and 16 kHz, there is a transition zone where strong mode changes were observed, and the displacement ratios do not correspond at all with the lever ratios for the LPM and NM. The latter ratios showed a hump of the same shape. For the umbo, the correspondence was better, but actual measurements should be made there to get the final answer. At frequencies above 17 kHz, the displacement ratios and lever ratios are very similar to the values below 10 kHz, but at frequencies above 35 kHz, the amplitude ratios steadily grow larger than the anatomical lever ratios, indicating that a smaller piston motion is imparted to the stapes than predicted by the lever model. For

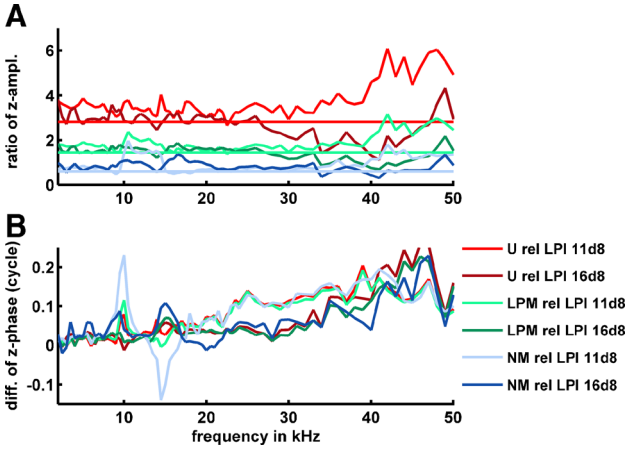

FIG. 16. The ratios of the *z* displacements of the U, LPM, and NM relative to the displacement at the LPI (the legend clarifies the line color codes.) for anesthetized animals 11d8 and 16d8 as a function of frequency. With the same color code, the ratio of the lever arms for each "observation" point was added as a *straight horizontal line*. The amplitude ratios for the different malleus points, shown in the *upper panel*, follow only approximately their lever arm ratio. Phase difference curves in the *lower panel* differ only in the frequency region 10–20 kHz. A gradual phase difference is developed between the three malleus points (U, LPM, NM) and the point at the LPI.

the 16d8 animal, the umbo/LPI ratio was relatively flat with values close to the lever ratio up to 27 kHz, then it dropped to smaller values up to 45 kHz and then increased again. The LPM/LPI and NM/LPI ratios were close to the anatomical lever ratios up to 35 kHz, with similarly shaped deviations to larger values in the 9 to 20 kHz range. The LPM/LPI ratio followed the trend of the umbo/LPI ratio at the highest frequencies, while the NM/LPI ratio stayed flat at the anatomical lever ratio level up to the highest frequencies.

There is also, however, a phase difference involved in the ratio of the displacements, which is depicted in Fig. 16B. This phase difference is mostly disregarded when lever ratios are presented (and in fact the lever ratio hypothesis implies that the phase difference must be zero). Up to 9 kHz, the phase differences for all points of the two animals are small and nearly the same. In the frequency region between 10 and 17 kHz, the phase differences between the three malleus points (umbo, NM, and LPM) and the LPI fluctuate for both animals. Above 17 kHz, the three phase differences for animal 11d8 are very similar and show an almost linear increasing trend; this holds also for animal 16d8, but the slope is smaller. At 35 kHz, the phase lead of the malleus points is about 0.15 cycle for animal 11d8 and 0.1 cycle for animal 16d8. Note that similar fluctuations in the same frequency range were seen in the phase difference between LPI and LPM from 1D experiments on gerbil with the same setup (Fig. 7, exp #59; de La Rochefoucauld et al. 2010).

Malleus and Incus Rotation About the Anatomical Axis

A more meaningful examination of the relative motion between incus and malleus can be made not by just looking at ratios of a few points on them but by comparing the rotation of the two ossicles about the anatomical axis. The choice of using the rotational components along the anatomical axis can be argued as follows. The piston component of the stapes has been shown to largely determine the pressure behind the footplate in the scala vestibuli (Decraemer et al. 2007). Given the anatomy of the ossicles and our choice of reference frame, this component is a result of rotation about the *x*-axis (the anatomical axis) and *y*-axis and translation along the *z*-axis (the stapes piston direction). Having made the choice of anatomical frame with the *x*-axis along the anatomical axis and the origin at the MIJ, we found that the translational components were all very small (as explained in the "THEORY" section, translating the *y*-axis to another location changes the *z* translation), so that rotation is the main determinant of the *z* displacement. Rotation about the *y*-axis will have a much smaller contribution because the rotation amplitudes of malleus and incus about the *y*-axis at most frequencies are about five times smaller than the corresponding *x* amplitudes (data for rotation in Figs. 7 and 8) and the perpendicular distance from the footplate center to the *y*-axis is about three times smaller than the distance to the *x*-axis (the *z* displacement contribution being the product of the two). Alternatively, one can easily check visually by looking directly at the motion of the ossicles (Figs. 9, 10, 11, 12, 13, 14, and 15A–C) that rotation about the *x*-axis is larger than rotation about the *y*-axis. The translation part of the displacements in the rigid-body description of the data has been found to be small at most frequencies; so it will provide only a small contribution to the total piston component. Last but not least, in Fig. 8, it was shown that the amplitudes for the *x* components of rotation were not only dominant but that the amplitude and phase of the malleus and incus *x* rotation components were very similar through the entire frequency range, while for the other components there was no such similarity. This means that *x*-axis rotation was transferred almost unaltered from malleus to incus.

In Fig. 17, the amplitude ratio (panel A) and phase difference (panel B) of the *x*-axis rotation components of the malleus with respect to those of the incus are shown for animals 9d8 (measured 5h PM), 11d8 (anesthetized), 16d8 (anesthetized), 16d8PM (animal

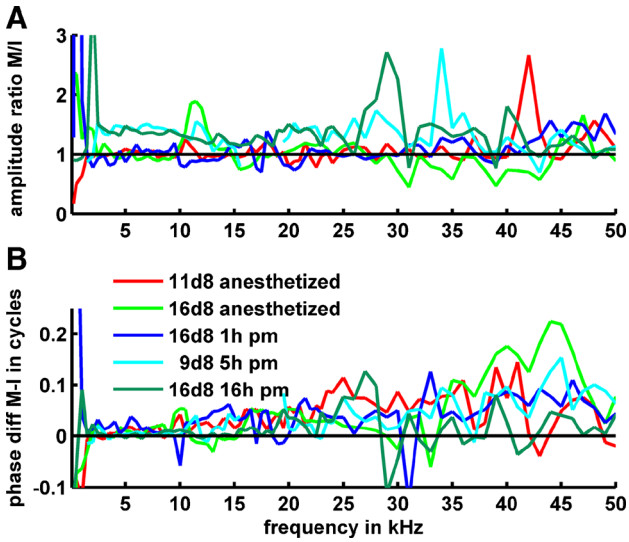

FIG. 17. The amplitude ratio of the malleus to incus (M/I, **A**) and phase difference between the malleus and incus (M-I, **B**) of the *x*-axis rotation components for observation in living and post mortem conditions: 9d8 measured in a 5h PM, 11d8 and 16d8 living-anesthetized, 16d8PM, the 16d8 animal 1h PM, and the animal of 16d8 16h PM. For the anesthetized animals (*red* and *light green*) and the 1h M animal (*blue*) he amplitude ratios are nearly equal to 1 from a few kilohertz up to 40 kHz (*red* and *blue*) or 30 kHz (*light green*), then there are some fluctuations (Fig. 19A). For the cadaver experiment, the amplitude ratio is on the average about 1.3 to 1.4 up to 35 kHz before dropping to about 1 at higher frequencies. Differences in phase between living and post mortem results were not prominent. The linear increasing trends in the phase differences are equivalent to time delays in the rotation from malleus to incus of about 2 to 3 μs, depending somewhat on the individual animals.

16d8, 1h PM), and 17d8 (animal 16d8, 16h PM). Let us again disregard the lowest frequencies, which display artifacts due to the PF opening. For the anesthetized animals (red and light green) and the 1h PM animal (blue), the amplitude ratios are nearly equal to 1 from a few kilohertz up to 40 kHz (red and blue) or 30 kHz (light green), then there are some fluctuations (Fig. 17A). For the 5-h and 1-day PM cadaver experiments (magenta and dark green), the amplitude ratio is higher than 1, on average about 1.3 to 1.4 with large variations up to 35 kHz, then it drops to about 1. From a few kilohertz on, small phase leads between malleus and incus (Fig. 17B) developed that showed a slowly increasing trend, again with large variations. No pronounced differences in phase were seen between living and post mortem results. There is an overall positive trend in the phase differences, equivalent to very small time delays in the rotation from malleus to incus (about 2 to 3 μs, depending somewhat on the individual animals), but the strong irregularities of the curves signify that we cannot speak of a constant delay.

We can conclude that when it comes to rotation about the anatomical axis (the rotation component of major importance), in anesthetized animals, the malleus and incus rotate with approximately the same rotation amplitudes and with a very small phase lag between them. Post mortem, the ratio of the rotation amplitudes of the malleus and the incus of animal 16d8 increased slightly for frequencies up to 35 kHz—this increase to about 1.3–1.4 on average was mainly caused by a post mortem decrease of the incus rotation amplitude that was larger than the decrease for the malleus (results of animal 16d8 alive and post mortem, not shown) while the phase relationship was not substantially altered. This decrease in amplitude might have been caused by a post mortem increase of the cochlear input impedance, perhaps due to stiffening of the annular ligament. Above 35 kHz, the difference in amplitude of the malleus and incus was less, so their ratio was again closer to 1.

Inertial Axes of the Ossicular Chain

When a body rotates about an axis of rotation that is aligned with one of the principal inertial axes of the body, the angular momentum vector is also aligned in the same direction and the rotation is stable. A well-known practical example of this mathematical phenomenon is the routine automotive task of balancing a wheel, which basically means adjusting the distribution of mass of a wheel such that its principal axis of inertia is aligned with the axle, so the wheel does not wobble. Setting the ossicular chain to rotate about an axis that is close to one of its principal axes would be a favorable situation, as it would tend to cause less stress in the supports and could be done with smaller torque.

An asymmetric object, such as the ossicular chain, has three principal inertial axes that are mutually orthogonal. For the 3D models of the ossicles used in the previous animation figures (Figs. 9, 10, 11, 12, 13, 14, and 15), we have calculated the principal inertial axes for the entire ossicular chain, considering it as one rigid block and assuming a uniform mass distribution. As the coupling between the incus and stapes is very flimsy at the region of the thin and flexible pedicle, we also considered a case where the stapes is disconnected from the malleus-incus block. In Fig. 18, both sets of principal axes are shown as red, green, and blue vectors originating from the center of mass of the total ossicular chain (black open circle, solid line vectors) or of the malleus-incus block (dashed line vectors), respectively. Three different views, along the *x*-, *z*-, and *y*-axes of the anatomical reference frame, are provided in panels A, B, and C. The moment of inertia about the red axis is the smallest, while that about the blue axis is the largest. Their lengths on the figure are equal, while their senses are chosen to let the red, green, and blue axes

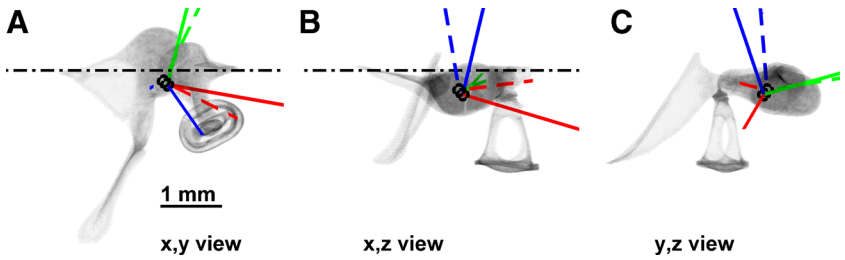

FIG. 18. The principal axes of the middle ear ossicular chain of gerbil, calculated as though the chain formed one solid block with uniform density, are shown as the *solid red, green,* and *blue vectors* anchored at the center of mass of the chain. The *dashed lines* represent the principal axes when the stapes is not included; they are anchored at the center of mass of the combined malleus and incus. The inertial axes form an orthogonal triplet. Three different views along the *x, z-,* and *y*-axes are provided from *left* to *right*. None of the three axes of both sets aligns well with the *x*-axis, the anatomical suspension axis. The moments of inertia about the principal axes increase from *red* to *green* to *blue*.

form a right-handed frame. None of the three principal axes in either set aligns closely with the anatomical suspension axis (*x*-axis, black dashed-dotted line); for the total chain, the red axis comes closest to it making an angle of about 10 ° with it in the *x*, *y* view and of about 20 ° with it in the *x*, *z* view. For the malleus-incus block, the angle is about 40 ° in the *x*, *y* view and about 10 ° in the *x*, *z* view. The centers of mass for the two sets are a few tenths of a millimeter away from the anatomical axis.

Alternatively, we can compare the location of the red principal axis with that of the TARAs for the different vibration modes shown earlier (Figs. 10, 11, 12, 13, 14, and 15). At the lowest frequencies shown, the positions of the TARAs of the malleus and incus were close to each other (Fig. 10 at 4.5 kHz and Fig. 11 at 7 kHz), and, here, we see that this position is also close to the solid red principal axis in the view of Fig. 18A (*x*, *y* view, the most commonly used experimental view, going through the ear canal), but this is not true for the other views in panels B and C. There is a somewhat better agreement at these lower frequencies between TARAs and principal axes when the malleus and incus are considered as one block: the direction of the red dashed axis is more slanted with respect to the *x*-axis (angle of ~40 °) than the TARAs of the malleus and incus in the *x*, *y* view (angle of ~10 °), but their directions compare rather well in the *y*, *z* view. At the higher frequencies (Figs. 12, 13, 14, and 15), the rotation axis varies strongly within the cycle and correspondences between the TARAs and the solid- or dashed-line principal axes were not observed.

We must therefore conclude that for gerbil, the ossicular chain is not really suspended along one of its principal axes nor is it vibrating about any of its principal inertial axes as was at one time hypothesized based on observations on human temporal bones (Kirikae 1960, p. 94). This indicates that to understand the vibration modes of the ossicular chain even at low frequencies, we cannot use an oversimplified model that makes abstraction of the refined connections of the ossicles with each other and with the other structures of middle ear such as the tendons and the tympanic membrane.

Complete Ossicular Motion (Model with Stapes Included)

As mentioned in the "Introduction to the Layout of the Plots Showing the 3D Motion of Malleus and Incus", it was not possible to find a data set for the stapes that matched the present malleus and incus motion at all frequencies. However, applying a single scaling factor to the translation displacement of the experiment 20m4 presented in Decraemer et al. (2007), we could nicely align the stapes motion with the incus motion of animal 11d8 for some low frequencies with rather simple vibration modes: at the incus-stapes joint (ISJ), the incus and stapes followed each other closely during the cycle. Because of the large inter-animal variability in high-frequency vibrations, we did not try to include stapes motion at other frequencies.

Figure 19 thus presents malleus and incus motion at 4.5 kHz for animal 11d8 combined with the stapes motion from experiment 20m4. (The malleus, incus, and stapes models are all from the same ossicular chain.) Six panels show the three ossicles in still frames of an animation at time instants 0, T/6, 2T/6, … 5T/6. The displacements were more strongly scaled up (by a factor of 30,000) than in the previous three-panel animation plots to make the relatively small stapes displacement more visible. In each panel, the rest position of the malleus and stapes is shown in gray; the rest position of the incus is not shown because it obscured what was happening in the LPI region.

One can observe a basic vibration mode with rotation of the malleus-incus block as was seen above (Figs. 10 and 11). With such a malleus-incus motion, the stapes is tilting about the long footplate axis while it is moving up and down; as a consequence, the angle between the long process of the incus and the plane of the crura of the stapes is changing slightly. This motion can be accommodated by a slight bending in the thin pedicle

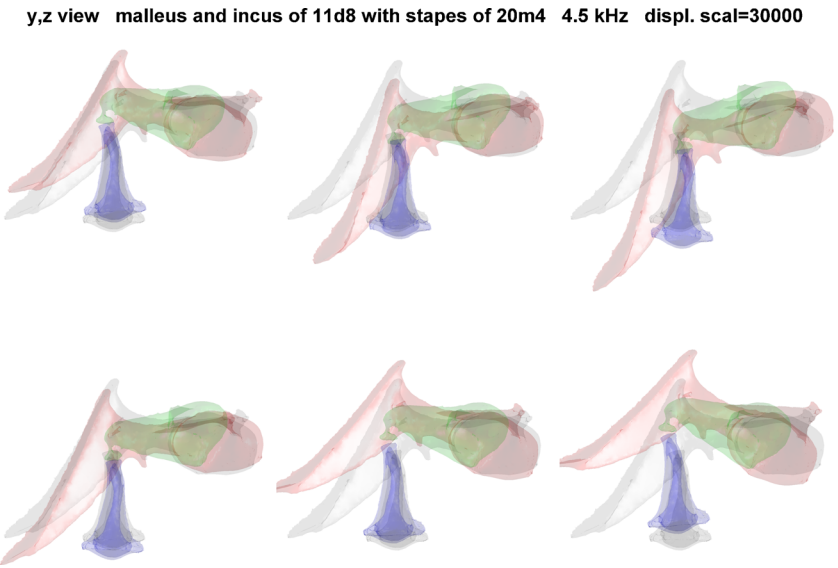

FIG. 19. Low-frequency vibration mode of the entire gerbil ossicular chain shown at six equally spaced instants of time in a cycle (sequence: *top panels left to right,* then *bottom panels left to right*). The displacements were scaled up by a large factor (30,000) to make the relatively small stapes displacement also visible. In each panel, the rest position of the malleus and stapes is shown in *gray*; the rest position of the incus is not shown as it obscured what was happening in the LPI region. For this plot, the malleus and the incus data of animal 11d8 at 4.5 kHz were complemented with data for the stapes at the same frequency from a previous experiment (animal 20m4; Decraemer et al. 2007). To align the data of the two animals, only a single amplitude scaling factor was used.

(Funnell et al. 2005) and some slippage in the ISJ in the direction of the short axis. A small rocking motion about the short axis was also seen (not shown here), perhaps related to a slight sideways slippage of the plate of the lenticular process relative to the head of the stapes in the direction of the long axis.

DISCUSSION

Mode of Vibration and Inter-Animal Differences

Examples of vibration modes for three animals (9d8, 11d8, and 16d8) were shown. The vibration modes for the three animals, measured in anesthetized or fresh cadaver conditions, are most similar in the frequency range between 2 and about 9 kHz, where modes that come closest to the classical rotation about the anatomical axis are seen. A close-to-perfect agreement was only seen in one animal, and only at a few frequencies. In the 10 to 15 kHz range, the vibration mode changed rapidly with frequency; in this frequency, range Figs. 7 and 8 show substantial changes in the relative magnitudes of the *x*, *y*, and *z* components of the translational and rotational displacement amplitudes. At higher frequencies, the modes changed more gradually: the rotation axis varies strongly within the cycle, TARAs of the malleus and incus do not align well with the *x*-axis (angles larger than 45 °) or with each other (angles of about 20 to 30 °). Large inter-animal differences are observed from 10 kHz on, which make it difficult to make a general statement about how the mode changes develop. Modes present in one animal in a given frequency range occur occasionally in a different range for another animal.

The strong changes in vibration mode that we observed in the 10–15 kHz frequency range can also be related to measurements of the 3D displacement of a single point on the posterior crus of gerbil presented by Ravicz et al. (2008). Variable magnitudes and phases of the transverse motions of this point were observed at all frequencies and especially "Between 9 and 13 kHz, transverse components in each ear were larger than those at other frequencies (in one ear, larger than the piston motion), and phase differences were more variable". As the deviation of the motion from the piston direction was within their error for the determination of the observation angle (20 °), they concluded that stapes motion was primarily piston-like to high frequencies except in the 9 to 13 kHz range. In the frequency range of 9 to 16 kHz, sudden changes in the amplitude ratio and phase difference between LPI and LPM were also found in results from 1D experiments on gerbil performed with the same setup as the one used here (Fig. 7, exp #59; de La Rochefoucauld et al. 2010).

Large inter-animal differences were encountered in the mode of middle-ear vibration of gerbil. This was also reflected in the same study as above by Ravicz et al. (2008; Fig. 5) who reported inter-animal differences of up to 20 dB in ossicular motion measured with a single-beam velocimeter at a point on the posterior crus in gerbil. Similar differences were seen

in measurements on the malleus and incus in gerbil reported by de La Rochefoucauld et al. (2010; Fig. 4).

Origin of Classical Ossicular-Motion Hypothesis

In a view along the ear canal, the TARAs at low frequencies are found to be almost parallel with the anatomical axis, but this is not at all true in the other views. Older experiments mainly used the ear canal approach. This, in addition to purely anatomical grounds, may be why the classical hypothesis of ossicular rotation about the anatomical axis, or an axis close to that, was formulated (for references see, e.g., Decraemer et al. 1991). When we look at the position of the instantaneous rotation point in our 1D analysis for low frequencies (the range for older experiments) shown in the left panels of Figs. 4 and 5, we see that it is situated at about 1.3 mm from the LPM and 0.9 mm from the LPI, which in the ear canal view of the ossicles in Fig. 2 correspond approximately to a position on the anatomical axis. Even when we consider high-frequency vibration modes, with 3D motions that are far from being a simple rotation, and apply a 1D analysis on a subset of that data observed on collinear points from a single observation direction (similar to what was done to check for rigidity of the ossicles), we get at many frequencies a surprisingly simple rotation image as illustrated in the right-hand panels of Figs. 4 and 5 showing high-frequency motion. (The simple rotation model does not hold well in the frequency range between 10 and 20 kHz as illustrated in the middle panel of Fig. 4 which shows a 1D analysis plot where in addition to rotation a substantial translation is present, pushing the instantaneous rotation axis far superior to the MIJ.) Remarkably, the apparently simple 1D observation can be in accord with a complex 3D motion; for example in Fig. 13, the instantaneous rotation axis changes strongly in direction during the cycle but this is in a nearly rotational motion about a point somewhere within the MIJ and as a result this motion closely resembles a simple rotation in a plot of a 1D analysis. Such a simple model, in accord with the obvious hinge-like suspension of the ossicles in the middle-ear cavity, had a long life till evidence became available that the motion was more complicated (e.g., Decraemer et al. 1994; Decraemer and Khanna 1999).

Three-Dimensional Ossicular Motion in Other Species

In addition to the gerbil, we have also studied the 3D motion in cat (Decraemer and Khanna 1999) and human (Decraemer and Khanna 2003). The low-frequency vibration mode observed for gerbil is comparable to what we have seen in cat. At higher frequencies for all species, the vibration mode became more complicated and more and more relative motion was seen in the MIJ and ISJ. The larger the ossicles are (they are smallest in gerbil, larger in cat, and largest in human), the larger the mass is, and, due to inertial effects (mass or inertial moments), it is reasonable to expect that the vibration mode will change at lower and lower frequencies. We indeed found that in human vibration, the mode started to become more complex at ~2 kHz, in cat around ~3 to 4 kHz, and in gerbil around 8 to 10 kHz.

At high frequencies, relative motion between the malleus and incus was prominent in all three species. For example, at certain frequencies, the cat malleus and incus rotated with opposite phase, resulting in a scissor-like motion that was not seen here. Slippage in human was so large that it looked as though a decoupling between malleus and incus took place and it is still hard to believe that this really happens in the healthy living ear. Indeed, in human, we could only perform measurements on temporal bones of elderly people (who mostly have high-frequency hearing loss which may involve a middle-ear component) and had to allow for post mortem delays of three to four days at the minimum (Decraemer and Khanna 2003). We measured five different temporal bones, and, in each case, the same phenomenon was observed: while the incus rotation was about 0.8 of the malleus rotation at low frequencies, it dropped sharply to about 0.15 of the malleus rotation above 2 kHz. Such large slippage between malleus and incus was also observed by Sim et al. (2003) and Willi (2002) in human temporal bone measurements. This was possibly a result of post mortem stiffening (e.g., of the annular ligament) although this is not supported by Chien et al. (2009) who did not find substantial differences in stapes motion between living human and temporal bone measurements. In gerbil, we also found that at 1-day post mortem, the incus mobility had decreased up to ~30 kHz. Above 30 kHz, the amplitude of the incus went back up, which could be explained by some decoupling between the incus and the very stiffly constrained stapes. Such a high-frequency region is of no importance for the human so no equivalent observation was ever made. Until further investigation, therefore, the question of whether the slippage effect seen in human ears is genuine or is a post mortem artifact remains open.

CONCLUSION

Three-dimensional measurements of the motion of the middle-ear malleus and incus in gerbil were successfully made in the present study. Up to 10 kHz, the mode of vibration was rather simple for all animals studied and resembled approximately a rotation about an axis in the neighborhood of, but not actually coinciding with, the

anatomical suspension axis of the malleus and incus running from the anterior mallear tip to the posterior incudal process. At higher frequencies, other rotation components joined in making the motion more complex: overall, we saw a rather consistent picture of rotations of the malleus and incus about individual axes that cross over in the neighborhood of the MIJ but that make substantial angles with each other and with the anatomical axis, but pronounced inter-animal differences were observed.

The mode of vibration of the gerbil middle ear resembles that of cat (Decraemer and Khanna 1999, 2003), but with differences. In cat, the slippage in the MIJ and changes in vibration mode at high frequencies were much more pronounced: at some frequencies, the LPM in cat had even larger motion amplitude than the umbo. In gerbil, the malleus and incus rotation components along the anatomical axis were found to be very similar in amplitude and phase throughout the entire frequency range (Fig. 17); this may be due to the fact that in gerbil the ossicles are smaller and lighter. The suspension of the anatomical axis is realized with soft tissue or very thin bone, so that some wobbling of the axis is to be expected, with changes of vibration mode with frequency as a result. Combining results from previous 3D vibration measurements on the stapes with the present results on the malleus and incus for a low-frequency rotational mode clearly showed a tilting of the footplate and a change in angle between the long process of the incus and the piston axis of the stapes that were also observed in cat and human (Decraemer and Khanna 1999, 2003).

With the present study, a complete view of gerbil ossicular motion is now available. The results may be used to validate mathematical models that can be used for further investigations where the middle ear is involved. The differences seen between 3D ossicular motion in gerbil, cat, and human are an indication that it is difficult to directly transfer experimental results from one animal model to another and, more importantly, from animal models to human. Detailed mathematical models such as finite element models can be used to understand the origin of these differences and can play an important role in transferring insights from the animal to the human ear.

ACKNOWLEDGMENTS

This work was supported by the NIH/NICDC (DC003130), the Emil Capita Fund, the Fund for Scientific Research (Flanders, Belgium), the Canadian Institutes of Health Research, and the Natural Sciences and Engineering Research Council of Canada. We thank N. Maftoon (Dept. BioMedical Engineering, McGill University) for checking our inertial axis calculations using Code_Aster. The first author would also like to thank R.D. Rabbitt for insightful discussions at a few meetings, many years ago, on the description of middle-ear motion using the rigid-body concept.

APPENDIX

The three components of the rotational displacement $d\boldsymbol{\theta}$ are harmonic functions of time.

With v representing the frequency, the x component, for example, can be written as

$$d\theta_x = d\theta_x^0 \sin(2\pi v t + \varphi_x) \tag{A.1}$$

where $d\theta_x{}^0$ is the amplitude and φ_x the phase constant of the x component.

If for $t=t_{max}$, the length of the vector $d\theta$ is maximal we have

$$d\theta_{x\max} = d\theta_x^0 \sin(2\pi v t_{\max} + \varphi_x) \tag{A.2}$$

Setting $\gamma_{max}=2\pi v t_{max}+\varphi_x$ and $\gamma=2\pi v(t-t_{max})$ we can rewrite (A.1) as

$$d\theta_x = d\theta_x^0 \sin[2\pi v(t-t_{\max}+t_{\max})+\varphi_x] = d\theta_x^0 \sin(\gamma_{\max}+\gamma) \tag{A.3}$$

where γ is the phase angle in the cycle relative to the phase angle γ_{max} at t_{max}.

The average of $d\theta_x$ in a symmetric interval $\pm\gamma_0$ around γ_{max} is calculated as $\overline{d\theta_x} = \frac{1}{2\gamma_0}\int_{-\gamma_0}^{+\gamma_0} d\theta_x^0 \sin(\gamma_{\max}+\gamma)d\gamma$ (A.3) or, expanding the sine function

$$\overline{d\theta_x} = \frac{1}{2\gamma_0}\int_{-\gamma_0}^{+\gamma_0} d\theta_x^0[\sin(\gamma_{\max})\cos(\gamma)+\cos(\gamma_{\max})\sin(\gamma)]d\gamma \tag{A.4}$$

$$\overline{d\theta_x} = \frac{d\theta_x^0 \sin(\gamma_{\max})}{2\gamma_0}\int_{-\gamma_0}^{+\gamma_0}\cos(\gamma)d\gamma + \frac{d\theta_x^0\cos(\gamma_{\max})}{2\gamma_0}\int_{-\gamma_0}^{+\gamma_0}\sin(\gamma)d\gamma \tag{A.5}$$

which yields

$$\overline{d\theta_x} = \frac{d\theta_x^0\sin(\gamma_{\max})}{2\gamma_0}[\sin\gamma_0-\sin(-\gamma_0)] - \frac{d\theta_x^0\cos(\gamma_{\max})}{2\gamma_0}[\cos\gamma_0-\cos(-\gamma_0)] = \frac{d\theta_x^0\sin(\gamma_{\max})\sin\gamma_0}{\gamma_0}$$

Using A.2 and the definition of γ_{max}

$$\overline{d\theta_x} = \frac{d\theta_{x\max}\sin\gamma_0}{\gamma_0} \tag{A.6}$$

This proves that $\overline{d\theta_x}$, the average value of $d\theta_x$ in the symmetric interval $-\gamma_0$ to $+\gamma_0$, is proportional to

the value of $d\theta_{x\ max}$. This holds for all three components so the time average value of the vector $d\boldsymbol{\theta}$ in a symmetric interval around t_{max} is parallel to the vector $d\boldsymbol{\theta}_{max}$.

The average value in the half cycle ($\gamma_0=\pi/2$) centered on the instant t_{max} (where the length of $d\boldsymbol{\theta}$ is maximal) is equal to $\overline{d\theta_x} = \frac{2d\theta_{xmax}}{\pi}$ (A.7)

This average takes into account all values of $d\boldsymbol{\theta}$ in the time interval within which the length of $d\boldsymbol{\theta}$ is increasing from minimal to maximal, and decreasing back again to minimal. In the following half cycle, the rotation of the body is reversed and so is the $d\boldsymbol{\theta}$ vector. The average of $d\boldsymbol{\theta}$ in a complete cycle is thus zero (cf. A.6, with $\gamma_0=\pi$, $\sin(\gamma_0)=0$).

REFERENCES

ANGELES J (1982) Spatial kinematic chains. Springer, Berlin

BOTTEMA O, ROTH B (1979) Theoretical kinematics. North-Holland Publishing, Amsterdam, also available from Dover Publications in 1990

CHIEN W, ROSOWSKI JJ, RAVICZ ME, RAUCH SD, SMULLEN J, MERCHANT SN (2009) Measurements of stapes velocity in live human ears. Hear Res 249(1–2):54–61

DE LA ROCHEFOUCAULD O, OLSON ES (2010) A sum of simple and complex motions on the eardrum and manubrium in gerbil. Hear Res 263(1–2):9–15

DE LA ROCHEFOUCAULD O, DECRAEMER WF, KHANNA SM, OLSON ES (2008) Simultaneous measurements of ossicular velocity and intracochlear pressure leading to the cochlear input impedance in gerbil. JARO 9:161–177

DE LA ROCHEFOUCAULD O, KACHROO P, OLSON ES (2010) Ossicular motion related to middle ear transmission delay in gerbil. Hear Res 270(1–2):158–172

DECRAEMER WF, KHANNA SM (1999) In: Rosowski JJ, Merchant S (eds) New insights in the functioning of the middle ear. Memro meeting 1999: The function and mechanics of normal, diseased and reconstructed middle ears. Kugler, The Hague, pp 23–38

DECRAEMER WF, KHANNA SM (2003) Measurement, visualization and quantitative analysis of complete three-dimensional kinematical data sets of human and cat middle ear. Proceedings of the 3rd Symposium on Middle Ear Mechanics in Research and Otology, Gyo et al (eds) World Scientific, 3–10 July 2003, Matsuyama, Ehime, Japan, 9–12

DECRAEMER WF, KHANNA SM, FUNNELL WRJ (1991) Malleus mode changes with frequency. Hear Res 54:305–318

DECRAEMER WF, KHANNA SM, FUNNELL WRJ (1994) Bending of the manubrium in cat under normal sound stimulation. In: Foth HJ et al (eds) Optical and imaging techniques. Proceedings of Progress in Biomedical Optics, Europto Series, 8–9 September 1994, vol 2329. Lille, France, pp 74–84, SPIE

DECRAEMER WF, DIRCKX JJJ, FUNNELL WRJ (2003) Three-dimensional modeling of the middle-ear ossicular chain using a commercial high-resolution x-ray CT scanner. JARO 4(2):250–263

DECRAEMER WF, DE LA ROCHEFOUCAULD O, DONG W, KHANNA SM, DIRCKX JJJ, OLSON ES (2007) Scala vestibuli pressure and three-dimensional stapes velocity measured in direct succession in gerbil. JASA 121:2774–2791

DONG W, OLSON ES (2006) Middle ear forward and reverse transmission in gerbil. J Neurophysiol 95(5):2951–2961

FUNNELL WRJ, SIAH TH, MCKEE MD, DANIEL SJ, DECRAEMER WF (2005) On the coupling between the incus and the stapes in the cat. JARO 6(1):9–18

KHANNA SM, KOESTER CJ, WILLEMIN JF, DÄNDLIKER R, ROSSKOTHEN H (1996) A noninvasive optical system for the study of the function of inner ear in living animals. SPIE 2732:64–81

KIRIKAE I (1960) Structure and function of the middle ear. The University of Tokyo Press, Tokyo

PRESS WH, FLANNERY BP, TEUKOLSKY SA, VETTERLING WT (1989) Numerical recipes. Cambridge University Press, New York

RAVICZ ME, COOPER NP, ROSOWSKI JJ (2008) Gerbil middle-ear sound transmission from 100 Hz to 60 kHz. J Acoust Soc Am 124(1):363–380

ROSOWSKI JJ, RAVICZ ME, TEOH SW, FLANDERMEYER D (1999) Measurements of middle-ear function in the Mongolian gerbil, a specialized mammalian ear. Audiol Neurotol 4:129–136

SALIH WHM, BUYTAERT JAN, AERTS JRM, VANDERNIEPEN P, DIERICK M, DIRCKX JJJ (2012) Open access high-resolution 3D morphology models of cat, gerbil, rabbit, rat and human ossicular chains. Hear Res 284(1–2):1–5

SIM JH, PURIA S, STEELE C (2003) Three-dimensional measurements and analyses of the isolated M-I complex. Proc. 3rd Symposium on Middle ear Mechanics in Research and Otolaryngology. Matsuyama, Japan, 61–67

WILLEMIN JF, DÄNDLIKER R, KHANNA SM (1988) Heterodyne interferometer for submicroscopic vibration measurements in the inner ear. JASA 83:787–795

WILLI UB (2002) The incudo-malleolar joint and sound transmission losses. Hear Res 174:32–44